ANL-7841

# CHEMICAL ENGINEERING DIVISION

# FUEL CYCLE TECHNOLOGY QUARTERLY REPORT

April, May, June 1971

D. S. Webster, A. A. Jonke,
G. J. Bernstein, N. M. Levitz, R. D. Pierce,
M. J. Steindler, and R. C. Vogel


ARGONNE NATIONAL LABORATORY, ARGONNE, ILLINOIS

Printed in the United States of America
Available from
National Technical Information Service
U.S. Department of Commerce
5285 Port Royal Road
Springfield, Virginia 22151
Price: Printed Copy $3.00; Microfiche $0.95

ANL-7841
Chemical Separations Processes
for Plutonium and Uranium

ARGONNE NATIONAL LABORATORY
9700 South Cass Avenue
Argonne, Illinois 60439

# CHEMICAL ENGINEERING DIVISION
# FUEL CYCLE TECHNOLOGY QUARTERLY REPORT

April, May, June 1971

by

D. S. Webster, A. A. Jonke, G. J. Bernstein,
N. M. Levitz, R. D. Pierce,
M. J. Steindler, and R. C. Vogel

August 1971

Previous reports in this series

ANL-7735, April, May, June 1970
ANL-7755, July, August, September 1970
ANL-7767, October, November, December 1970
ANL-7799, January, February, March 1971

TABLE OF CONTENTS

## LIST OF FIGURES



## LIST OF TABLES

# FUEL CYCLE TECHNOLOGY QUARTERLY REPORT

April, May, June 1971

by

D. S. Webster, A. A. Jonke, G. J. Bernstein,
N. M. Levitz, R. D. Pierce,
M. J. Steindler, and R. C. Vogel

## ABSTRACT

During the period April through June 1971, work was done in the following areas: (1) development of zinc decladding and melt decladding processes for the preparation of steel-clad LMFBR oxide fuel for acid dissolution, (2) study of the crystallization behavior of uranyl nitrate-plutonium nitrate-nitric acid solutions under consideration as feed solutions for a fluidized-bed process to prepare U-Pu oxides from their nitrates by denitration, (3) initial runs with uranyl nitrate to study the operability of a new denitration pilot plant, (4) evaluation of the precision of an X-ray fluorescence analytical method for determining Th/U ratio in $ThO_2$-$UO_2$ (a stand-in for $UO_2$-$PuO_2$), and (5) continued investigation of the performance characteristics of a centrifugal contactor for the plutonium isolation steps in the solvent extraction of LMFBR fuels.

## SUMMARY

### I. Liquid-Metal Decladding of Reactor Fuels

Liquid-metal head-end processes are being developed at Argonne to provide relatively simple and inexpensive techniques for reprocessing LMFBR fuels in aqueous-solvent extraction plants.

In one liquid metal process being studied, the fuel cladding is removed by dissolution in liquid zinc at 800°C, after which the steel-zinc solution is removed from the process vessel. Next, the fuel oxides, which do not react with the zinc and remain in the process vessel, are reduced to metal with a liquid Mg-Zn-Ca alloy in the presence of a salt phase. After this reduction step, the liquid metal alloy is retorted to concentrate the uranium and plutonium for nitric acid dissolution and further purification by solvent extraction. During decladding, all of the sodium, iodine, and fission-product gases are easily and efficiently separated from the fuel. Xenon and krypton are collected as a concentrated gas mixture, and all other process wastes are discharged as compact solids that have good heat-transfer properties.

Melt decladding is another liquid-metal head-end process under study. The fuel oxide is declad by melting both the stainless steel cladding and the subassembly structural members and draining part of the molten steel away from the fuel. Melt decladding avoids all mechanical dismantling of the fuel, allows the liberated fission gases and iodine to be collected,

and removes sodium from the fuel. However, the iodine and fission gases that are contained in the oxide matrix are not separated from the fuel by this process.

Engineering Development of Zinc Decladding

In the zinc-decladding, oxide-reduction scheme, the stainless steel cladding is dissolved in zinc, then the zinc-steel slurry is transferred out of the tungsten vessel to separate it from the fuel oxide. It is proposed to concentrate this waste by distilling away the zinc if this should prove economically attractive. The use of still pots of mild steel for the zinc evaporation step is being considered. The steel-saturated slurries from several decladding cycles might be retorted in the vessel, which would be the permanent storage container for the waste stainless steel.

To evaluate the corrosion of steels by zinc-stainless steel slurries, 4-in. lengths of 3/8-in. black iron pipe were exposed for 1 hr to a Zn-20 wt % stainless steel slurry at temperatures up to 850°C. After exposure, the pipe segments showed no detectable corrosion. Evaluation of mild steel crucibles for retorting of zinc-steel alloys has been started.

In another investigation, modifications of the metal-salt reduction system used to reduce the fuel oxide are being studied. As reported previously, pressed-and-sintered $UO_2$ pellets have been completely reduced in less than 4.5 hr by stirring the fuel oxide with a system consisting of a $CaCl_2$-20 mol % $CaF_2$ salt and either of two alloys--64 at. % Zn-29 at. % Mg-7 at. % Ca or 17 at. % Zn-79 at. % Mg-4 at. % Ca. Since any reduction salt entrained with the uranium-plutonium alloy would cause corrosion problems if introduced into the aqueous fuel recovery process, techniques for removing the salt are being studied. Retorting studies showed that $CaCl_2$ would be removed in the step in which the reduction product alloy is retorted to concentrate the uranium and plutonium. Since $CaF_2$ is not sufficiently volatile to be evaporated at the conditions used in retorting, the possibility of using reduction salt containing no $CaF_2$ is under study.

Two successful reductions of $UO_2$ pellets have been made with the high-zinc reduction alloy and a salt phase containing only $CaCl_2$; two reductions with the low-zinc alloy and $CaCl_2$ resulted in only 98 and 99% of the $UO_2$ being reduced in 4.5 hr.

Another possible modification of the salt-metal system is related to the requirement that iodine released during decladding be retained in the melt. Any elemental iodine released reacts with zinc in the melt to form $ZnI_2$, which collects primarily in the salt layer. The addition of KCl to the salt is being considered because in its presence the vapor pressure of $ZnI_2$ over the salt phase is reduced considerably. Because the salt from the decladding step also enters the reduction step, the effect of KCl on the $UO_2$ reduction rate is being investigated. With a $CaCl_2$-25 mol % KCl salt phase, reductions were incomplete with both the high- and low-zinc reduction alloys. These poorer reductions may have resulted from a lower solubility of CaO in the $CaCl_2$-KCl salt than in $CaCl_2$.

Data were needed on the rate of dissolution in nitric acid of U-Pu alloys obtained by retorting the uranium-plutonium-magnesium-zinc-calcium alloys produced in the reduction step. Small ingots (1.5 to 3.3 g) of U-Pu alloys were prepared and treated with boiling concentrated $HNO_3$. Alloys containing 1.6 and 9.7% plutonium dissolved readily, but alloys containing 64 and 91% plutonium were not completely dissolved. These data indicate that U-10 wt % Pu, the expected product of corecovery of uranium and plutonium, can be dissolved in concentrated $HNO_3$ for subsequent feeding to the solvent extraction process.

Process Demonstration Experiments

The zinc head-end process will be demonstrated by processing stainless steel-clad $UO_2$-$PuO_2$ fuel pins that were irradiated in EBR-II to a burnup of ∿3.3 at. %. The experimental apparatus for this investigation has been installed in the shielded facility and has been tested with a simulated fuel pin containing unirradiated $UO_2$ pellets.

Melt Decladding

The last of a series of scouting experiments to explore various schemes for melt decladding has been completed. Experiments during this period were related to a concept in which the subassembly is lowered slowly into a furnace so that the steel melts and the steel and fuel pellets fall onto a cooled surface. The larger pieces of steel are removed from the fuel (e.g., by screening), and the oxide along with associated steel may be fed to an acid dissolver.

In the melt decladding experiments, a small, simulated subassembly was lowered vertically into an induction-heated zone. Material falling from the hot zone fell through a 6-in.-long unheated zone and onto an inclined cold steel tray. When molten steel drops struck the tray, they formed thin flat plates and about 10% fines. At the end of an experiment, a few sections of unmelted cladding were found, but all the $UO_2$ pellets were observed to be exposed for subsequent acid dissolution.

The results of these experiments and other results reported earlier will be used to prepare preliminary designs of various melt-decladding concepts. A process design is described in this report in which the molten steel and the pellets are poured from a crucible into separate containers.

## II. Continuous Conversion of U/Pu Nitrates to Oxides

A continuous fluidized-bed denitration process is under development for converting uranyl nitrate-plutonium nitrate solutions to mixed oxides suitable for the fabrication of fuel shapes.

Earlier studies of the cosolubility of uranyl nitrate hexahydrate (UNH) and plutonium nitrate in dilute nitric acid solutions were extended in order to identify the crystallized phases. This information is pertinent to the selection of the feed solution composition for the fluid-bed denitration process since the feed solution should be as concentrated as

possible to increase throughput but not so concentrated that inadvertent crystallization of plutonium nitrate occurs. In current work with solutions containing 1.4-2.0M (U+Pu) and U/Pu ratios of 1 to 4, uranyl nitrate was the crystallizing phase, even from solutions with a U/Pu ratio of 1. Plutonium contamination of the crystallized phase was attributed mainly to an adsorption phenomenon. A separate study showed that the valence of plutonium in such solutions did not affect the crystallization temperature; a solution containing a mixture of hexavalent and tetravalent plutonium was found to have about the same crystallization temperature as a solution containing only tetravalent plutonium.

Most of the modifications of the denitration pilot plant necessary for work with plutonium have been completed. Major changes included the installation of the dissolver, feed storage vessel, and feed metering tank, which comprise the feed makeup system. The fluidized-bed denitration unit was provided with a larger opening at the bottom to facilitate solids removal.

The first run (U-7) of several new shakedown runs with uranyl nitrate was made in the pilot plant. In the course of preparing a 50-liter batch of 1.9M UNH feed solution with 1.4M excess $HNO_3$ for run U-7, the feed makeup system functioned well. The fluidized-bed denitration unit was operated for 10.5 hr in Run U-7. The run was performed at 300°C with a fluidized bed of $UO_3$, a feed rate of 95 ml/min for the bulk of the run (consuming the entire batch of feed solution), and an inlet gas flow corresponding to a superficial linear velocity of about 0.9 ft/sec (at column temperature and pressure).

The product-removal system (for continuous removal of $UO_3$), consisting of a sidearm for bed overflow and a collection reservoir, functioned well except for the last two hours when unexplained blockage of the sidearm occurred. During the final period, product was removed through the valve at the bottom of the unit. A uniform bed level was maintained during the entire run. The peak $UO_3$ production rate (during the last 7 hr of the run) corresponded to 80 lb/(hr)(sq ft reactor cross section).

Sieve analyses of hourly product samples and of a sample of the final bed established the nature of particle size distribution changes. Coarse material (+10 mesh) equivalent to about 3% of the $UO_3$ produced was found in the final bed; some of the large particles, obviously formed on the spray nozzle, were as large as 1 in. across. Accumulation of this amount of coarse material in the bed did not affect the operation of the denitrator. Sieve analyses showed that average bed particle size increased initially and then gradually decreased during the 10.5-hr period. Firm conclusions regarding particle size distribution trends cannot yet be made because of the limited duration of the run.

## III. In-Line Analysis in Fuel Fabrication

X-ray fluorescence (XRF) is being studied as a method for analysis of plutonium content in oxide fuel, utilizing $ThO_2$-$UO_2$ mixtures as a stand-in for $UO_2$-$PuO_2$. Work is being done to determine whether the relative standard deviation of ±0.5% desired for plutonium analysis can be achieved in analyzing mixed-oxide fuel materials. Count rates obtained from pellets

and powders of $ThO_2$-$UO_2$ have been subjected to an analysis of variance, in which it was assumed that the errors of the method and counting statistics are independent and that the variances are additive.

Four pellets were prepared from each of the following powders: pure $UO_2$, $ThO_2$-10 wt % $UO_2$, $ThO_2$-20 wt % $UO_2$, and $ThO_2$-30 wt % $UO_2$. Five measurements were made on each pellet. The variability of measurements on the same pellet was determined and attributed to the method; the variability of different pellets of the same nominal composition was determined, and the variability in excess of that attributable to the method was attributed to material effects.

The relative standard deviation due to the XRF method was adequately low, 0.48% at the 95% confidence level. A greater variability was observed between samples of $ThO_2$-30 wt % $UO_2$ powder than between samples of $ThO_2$-30 wt % $UO_2$ pellets. This indicates a potential problem due to mixing, blending, sampling, or material properties.

## IV. Adaptation of Centrifugal Contactors in LMFBR Fuel Processing

The performance characteristics of a centrifugal contactor suitable for use during plutonium purification in the Purex-type solvent extraction of LMFBR fuel material are being investigated. In such contactors, criticality hazards caused by high plutonium concentrations in the process streams will be controlled by limiting the diameter of the contactor to geometrically favorable dimensions. The unit is made of stainless steel and has a hollow rotor with a 4-in. ID and a 15-in. length, including a 12-in. long settling zone.

Tests have been made with aqueous and organic solutions at operating speeds between 2000 and 3500 rpm to measure separating capacity; separating capacity is defined, arbitrarily, as the throughput at a maximum of 1 vol % cross contamination of one phase by the other. The aqueous phase consisted of 0.5M $HNO_3$; the organic phase consisted of 15 or 30% tributyl phosphate in Ultrasene (refined kerosene). For all rotor speeds, capacities were lowest at aqueous-to-organic (A/O) flow ratios near 1 or 2 and were higher at higher and lower A/O ratios. At a rotor speed of 3500 rpm, separating capacity ranged from 8 to 17 gpm and varied with solution composition and A/O ratio. Based on past performance of other centrifugal contactors, a capacity of approximately 10 gpm (within a factor of two) had been predicted for the ANL unit.

Flow surging, reported previously, again occurred during high-speed operation and was attributed to excessive pumping characteristics of the mixer assembly. Surging was eliminated by bleeding air at a rate of 0.2-0.3 cfm into the tee at the entrance of the aqueous-organic mixing chamber. Thereafter, mechanical operation during the tests was satisfactory.

Performance of the unit to date demonstrates that small-diameter long-rotor contactors can be operated stably at high speed and have high capacity. Factors related to critical speed and dynamic balance have to be carefully considered in the design of such units.

## V. The Electrolytic Reduction and Reoxidation of Plutonium in Purex Processes

Engineering design studies have been made for application of electrochemical reduction of plutonium to Purex processing of LMFBR fuel. In the preliminary studies, pertinent electrochemical technology and also specific experimental results of similar electrochemical reductions of uranium have been reviewed and analyzed. From these analyses, quantitative models were established to relate process variables and design parameters for optimization of equipment design. Emphasis was placed on the design of a cathode chamber and a diaphragm for a steady-state flow system.

Interim reference designs, one with a plate-type cathode and one with a wire-screen cathode, were developed for a continuous-flow electrochemical reduction unit to be operated at rates up to 500 kg plutonium per day. A high degree of compactness, short residence time, and low pressure drop can be embodied in this unit. The holdup volume of a unit is about 3 1/2 liters at 50% reduction efficiency. It is visualized that several such units would be used in conjunction with a bank of centrifugal contactors.

In the course of these studies, detailed analyses were made of mass transfer and general flow behavior in electrochemical cells. Electrochemical techniques offer relatively direct, more convenient methods of measuring mass transfer, turbulence, and mixing behavior in the liquid phase than do other techniques.

# I. LIQUID-METAL DECLADDING OF REACTOR FUELS
(R. D. Pierce)

Liquid-metal decladding processes under development at Argonne appear to provide relatively simple and inexpensive techniques for solving formidable head-end processing problems related to the high burnups, short cooling times, and residual sodium of irradiated LMFBR fuels.

Early LMFBR fuel elements will consist of mixed uranium and plutonium oxides jacketed in stainless steel tubes. Following irradiation, these fuels may be allowed to decay for as little as 30 days. The localized heat generation in LMFBR fuels is very high, creating heat-dissipation problems during handling and processing operations.

High concentrations of radioactive iodine (especially $^{131}I$), xenon, and krypton in spent LMFBR fuel will present serious problems in handling and disposing of the waste-gas effluent from reprocessing operations. To avoid excessive emissions of highly radioactive isotopes such as $^{131}I$ to the environment, head-end operations must be performed in a sealed cell, and fission gases must be contained efficiently. If possible, the volatile elements should be removed from the fuel material prior to the nitric acid dissolution step of aqueous fuel processing.

If sodium is present in failed fuel elements, it too could present cleaning and fuel-dissolution problems since sodium can react explosively with nitric acid. In addition, the high plutonium content of LMFBR fuel presents criticality problems.

In one scheme for liquid-metal decladding, cladding is removed by immersing all of the fuel region of a discharged fuel subassembly in a pool of molten zinc having a molten-salt cover layer. (Probably, the bottom of the fuel subassembly would be cropped prior to immersion.) The zinc dissolves the stainless steel components (i.e., the subassembly supporting members and the cladding), but does not react with the fuel oxides. The resulting zinc solution is then removed from the decladding vessel to separate it from the fuel oxides. The fuel oxides are next reduced to metal with Mg-Zn-Ca alloy in the presence of a salt phase. Depending on whether the Mg-Zn-Ca alloy has a high or low zinc concentration, the uranium and plutonium are removed from the decladding vessel in the same liquid-metal solution or in separate liquid-metal solutions. After evaporation of the solvent metals, the reduced fuel is dissolved in nitric acid for further purification. During the decladding and reduction steps, all of the sodium, iodine, and fission-product gases are removed from the fuel.

Advantages of decladding in molten zinc include (1) efficient removal and collection of iodine and other volatile fission products, (2) relative ease of dissipation of fission-product heat, (3) elimination of the requirement for separate sodium-removal steps, (4) discharge of all process waste streams (except xenon and krypton) as solids having good heat-transfer properties, (5) collection of xenon and krypton in an inert cover-gas mixture (containing ~50% Xe plus Kr) of small enough volume (i.e., with

minimum dilution) to allow storage in gas cylinders, and (6) process simplicity and flexibility.

The principal disadvantages of liquid-metal decladding are a lack of industrial experience in the use of refractory metals and graphite as materials of construction, and the need to dispose of large quantities of reagent salt as waste. Although refractory metals and graphite are compatible with liquid zinc and molten salts and although equipment items fabricated of these materials have long lives, their cost is a significant portion of the processing cost. About 20 $ft^3$ of salt is used for each ton of fuel processed. However, solid salt is a convenient waste form, and the reagent and waste-disposal costs are not large. (The zinc and magnesium reagents are recovered by a vacuum-vaporization process for recycle.)

Another scheme for liquid-metal decladding utilizes direct melting of the stainless steel cladding and subassembly supporting members. A major portion of the molten steel can be separated from the fuel and cast into a waste ingot; the steel still associated with the fuel can be charged with the fuel to either an acid dissolution step or a voloxidation step to complete the separation of steel from fuel. Melt decladding avoids mechanical dismantling of the fuel, allows liberated fission gases to be collected in a compact form, evaporates residual sodium from the fuel, provides a compact waste, and adds no extraneous metal to the fuel before it is fed to the acid dissolution step. The major difficulties of the step are high temperature (>1450°C), relatively poor separation of steel from oxide, difficulties in handling the declad fuel, and low removal of iodine from the fuel.

A. Engineering Development of Zinc Decladding (I. O. Winsch, T. F. Cannon, J. J. Stockbar)

As described above, the first step in one procedure proposed for liquid-metal decladding is to dissolve stainless steel cladding by immersing fuel subassemblies in molten zinc having a molten-salt cover layer. The melt is contained in a tungsten decladding vessel at 800°C. The zinc-steel solution thereby produced is transferred out of the vessel away from the fuel. An alloy of Mg-Zn-Ca and additional salt are added to the fuel oxide and salt in the decladding vessel.

By contacting the oxide fuel with the molten metal/salt system, the fuel oxide is reduced to metal and dissolved in the reduction alloy. Two schemes for reducing fuel oxides are proposed. In one, which employs a high-zinc reduction alloy, both the plutonium and uranium products are in solution in the liquid metal. In the other, which employs a low-zinc reduction alloy, the plutonium is in solution in the liquid metal and metallic uranium precipitates. In the latter scheme, the uranium precipitate is subsequently dissolved in another metal alloy after the plutonium-bearing solution has been transferred out of the reaction vessel. Flowsheets for the two cases were presented in the preceding report in this series, ANL-7799, pp. 14-17.

The salt from the reduction step becomes a waste stream, and the metal phase containing the reduced fuel, which is the head-end product,

may be pressure-transferred out of the reaction vessel. The product solution is further concentrated by evaporating away all or part of the solvent alloy prior to dissolution of the metallic fuel in nitric acid for aqueous solvent extraction processing.

In the reduction procedure, all iodine would be released and collected in the waste salt and all gaseous fission products would be released in the sealed decladding furnace and collected for storage with minimum dilution by other gases.

1. Zinc Distillation

In the conceptual zinc head-end process for LMFBR fuels, the stainless steel cladding is dissolved in a zinc solution and the zinc-steel slurry is transferred to a separate vessel. It is proposed to concentrate the waste steel in this slurry by evaporating the bulk of the zinc, which would be recycled. A vacuum retort used in laboratory investigations of the Skull Reclamation Process, a pyrochemical process,[1] is being reassembled for use in studying the removal of zinc from waste solutions and the preparation of waste steel for disposal.

The vessel used to collect the zinc-steel solution from decladding would also serve as the still pot in the evaporation step. Since it would be difficult to remove the steel from the still pot following evaporation, consideration is being given to using the distillation vessel as the ultimate waste container as well. It might be used for several cycles of collecting zinc-steel slurry and evaporating zinc before enough steel is collected to warrant disposal of the vessel as a sealed container. Since the waste zinc slurry will be saturated with iron from the stainless steel and since nickel leaching of a mild-steel crucible would not occur, the zinc is not expected to be very corrosive to mild steel. Therefore, a mild steel crucible is being considered for the zinc evaporation step.

A run (ZDS-15) was made to evaluate the corrosion of steel pipe by a zinc solution that contained about 20 wt % stainless steel. Four-inch lengths of 3/8-in. black iron pipe were exposed for 1 hr each to the zinc-steel slurry, which was agitated gently. Samples were exposed at 750, 800, and 850°C. Following exposure, the pipe was sectioned and examined metallographically; there was no detectable attack on any sample.

Crucibles of mild steel will be used in the evaporation studies, and any effects of thermal gradients on corrosion will be sought. The rate of zinc evaporation, the character of the residue, and the performance of the crucibles will be determined.

2. Reduction of $UO_2$ Pellets

In the reduction step that follows zinc decladding in the proposed liquid-metal head-end process, declad oxide fuel is contacted with a liquid salt and molten-metal alloy containing a reductant. With adequate stirring of the fuel oxide, salt, and alloy phases, the $UO_2$ and $PuO_2$ are converted to metal, and the reduced plutonium is dissolved in the liquid-metal solution. Depending on the composition and quantity of the reduction alloy, the reduced uranium may be dissolved in the liquid-metal solution, precipitated, or

partially dissolved.

As described in the previous report in this series (ANL-7799, pp. 15-20), two metal-salt systems have been used successfully for reduction of $UO_2$ pellets ($UO_2$ is more difficult to reduce than is $UO_2$-$PuO_2$): 17 at. % Zn-79 at. % Mg-4 at. % Ca/80 mol % $CaCl_2$-20 mol % $CaF_2$ and 64 at. % Zn-29 at. % Mg-7 at. % Ca/80 mol % $CaCl_2$-20 mol % $CaF_2$. The former alloy, which is low in zinc, dissolved plutonium but has a low solubility for uranium; the latter alloy, which is rich in zinc, dissolves both uranium and plutonium. With either system, it is proposed to concentrate the product solution by vacuum evaporation prior to acid dissolution of the plutonium or uranium-plutonium alloy; zinc and magnesium condensate from this step would be recycled.

Some salt may be entrained with the reduction alloy fed to the zinc-magnesium evaporation step. Although $CaCl_2$ would be removed during vacuum evaporation (as is discussed below), $CaF_2$ is not sufficiently volatile to be removed and would enter the dissolver solution. Since fluoride ion in acid solution may cause corrosion problems in aqueous processing, the possibility of eliminating $CaF_2$ and using only $CaCl_2$ as the salt is under study.

An earlier run Mg-Zn-11 (ANL-7799, p. 19) showed that $UO_2$ pellets can be reduced readily and completely at 800°C in a high-zinc, fluoride-free system: 65 at. % Zn-29 at. % Mg-6 at. % Ca/$CaCl_2$. However, in that run, the salt and metal phases did not separate well following the reduction step--many metal droplets remained uncoalesced near the metal-salt interface. It has now been demonstrated that these droplets will coalesce if a short period of gentle agitation is provided following the vigorous mixing used to promote reduction.

Additional runs with $CaCl_2$ as the salt phase have been made to investigate (1) the extent of reduction with both high- and low-zinc alloys and (2) the $UO_2$ loading in the salt phase. Excellent reduction was obtained at 825°C in run Mg-Zn-18 which, like Mg-Zn-11, used a high-zinc, fluoride-free system and a salt-to-$UO_2$ ratio of 5. Two attempts (runs Mg-Zn-15 and -19) to reduce $UO_2$ pellets with a low-zinc/$CaCl_2$ system and a salt-to-$UO_2$ ratio of 5 at 810-830°C were less successful (99 and 98% reduction in 4.5 hr). This potential loss of 1 or 2% of the fuel is not considered acceptable.

In work using less salt (salt-to-$UO_2$ ratio of 1.7) and a 80 at. % Mg-12 at. % Zn-8 at. % Ca/$CaCl_2$ system at 810°C, reduction was only 50% complete in 4.5 hr (run Mg-Zn-14). A comparable low-zinc run* using $CaCl_2$-$CaF_2$ salt (run Mg-Zn-12) had been successful. Thus, only the high-zinc alloy has given good reductions with the fluoride-free $CaCl_2$.

---

*The salt-to-$UO_2$ ratio in run Mg-Zn-12 (erroneously indicated to be 5 in ANL-7799, p. 18) was 1.7. Thus, Mg-Zn-12 and -14 were performed at similar conditions.

The results reported above indicate that the use of $CaCl_2$ as the salt for reduction puts a constraint on the $UO_2$ loading in the feed and on the reduction temperature. One of the products of the reduction is CaO. The equilibrium solid phase for the $CaCl_2$-CaO system is CaO at temperatures above 835°C, but is CaO·2 $CaCl_2$ below 835°C. To avoid the precipitation of the latter voluminous material, it is necessary to restrict the $CaCl_2$-to-$UO_2$ weight ratio to values above ∿5 when the reduction temperature is below 835°C so that CaO will remain dissolved in the salt. Above 835°C, the use of less salt may be feasible.

Another possible modification of the salt system is related to the requirement of complete retention in the melt of the iodine released during decladding. The $ZnI_2$, formed when the iodine vapor rises through the molten zinc, is scrubbed out during passage through the overlying salt layer. Dilution of the volatile $ZnI_2$ with $CaCl_2$ decreases the vapor pressure of $ZnI_2$, and the vapor pressure can be further diminished, for better retention, by complexing the zinc. Complexing of zinc ions as $ZnCl_4^{-2}$ has been shown to be promoted by the presence of KCl (ANL-7755, p. 37). Consequently, use of a $CaCl_2$-KCl salt is also being considered for the decladding step of the zinc head-end process (this salt will also enter the reduction step). Another advantage of using $CaCl_2$-KCl is that its lower melting temperature would make phase-transfer difficulties in the reduction step less likely.

In one laboratory-scale reduction, 75 mol % $CaCl_2$-25 mol % KCl was used at 800°C with a low-zinc alloy (84 at. % Mg-13 at. % Zn-3 at. % Ca) at 800°C (run Mg-Zn-16); the ratio of salt to $UO_2$ was 5. Reduction was only 94% complete after 3.5 hr, in contrast to 99% in the comparable run Mg-Zn-15 in which $CaCl_2$ was employed. A $CaCl_2$-KCl run (Mg-Zn-17) was made with a high-zinc alloy (64 at. % Zn-30 at. % Mg-6 at. % Ca) at ∿830°C with a salt-to-$UO_2$ ratio at 5; reduction was only 89% complete after 5 hr. In the comparable $CaCl_2$ runs (Mg-Zn-11 and -18), reduction was essentially 100% complete. The poorer reductions in Mg-Zn-16 and -17 may have resulted from a lower solubility of CaO in the mixed salt than in $CaCl_2$. Although KCl is desirable in the decladding step, its concentration in the larger quantity of salt used for the reduction step will have to be kept low.

3. $CaCl_2$ Distillation Rate

To determine whether $CaCl_2$ accompanying the Zn-Mg-U-Pu alloy to the evaporation step would be removed at an adequate rate with zinc and magnesium, the evaporation rate for $CaCl_2$ at 0.07 Torr was measured. The rate ranged from 15 g $hr^{-1}$ $cm^{-2}$ at 1200°C to 0.45 g $hr^{-1}$ $cm^{-2}$ at 1000°C. These rates are more than adequate to assure that any $CaCl_2$ present would be removed in the evaporation step.

4. Dissolution of Uranium-Plutonium Alloys

Four experiments were done to evaluate the suitability of the product of the Zn-Mg evaporation step as feed for the following step, in which the alloy will be dissolved in $HNO_3$. (A 10% plutonium alloy would be produced from proposed core fuel elements by co-recovery of uranium and plutonium with a zinc-rich alloy; a high-plutonium alloy would be produced in the head-end step by use of a magnesium-rich alloy.) Since no applicable

dissolution data were found, an attempt was made to prepare several small ingots of selected compositions for dissolution tests. The uranium and plutonium did not alloy well; the charges apparently were too small to flow and coalesce. Four small ingots that had coalesced partially were treated with boiling, concentrated nitric acid. These ingots ranged from 1.5 to 3.3 g and contained 1.6, 9.7, 64, and 91% plutonium.

Alloys containing 1.6 and 9.7% plutonium were readily dissolved in boiling concentrated $HNO_3$, but dissolution of the plutonium-rich alloys was incomplete. These data indicate that solubility of a 10% plutonium-uranium alloy in concentrated nitric acid is adequate but that difficulty would be encountered in dissolving high-plutonium alloys in nitric acid.

B. Process Demonstration Experiments (T. R. Johnson, W. A. Murphy, R. W. Clark)

Experimental apparatus for the investigation of the zinc head-end process with 100 g of irradiated fuel has been installed in the shielded cell and has been tested in an experiment with a simulated fuel pin containing unirradiated $UO_2$ pellets.

In this experiment, 100 g of pressed and sintered $UO_2$ pellets (0.21-in. OD by 0.25-in. long, 90% of theoretical density) were placed in a Type 316 stainless steel tube that had a 0.25-in. OD and a 0.016-in. thick wall. This simulated fuel pin was placed in a perforated tantalum basket and immersed in zinc at 800°C. Overlying the molten zinc was a salt layer having the composition 90 mol % $CaCl_2$-10 mol % $CaF_2$. After the cladding was dissolved in the molten zinc, the basket containing the pellets was removed. Magnesium and $MgCl_2$ were added to the zinc to reduce and dissolve any $UO_2$ that had escaped from the basket during decladding.

After the top of the basket was plugged with a piece of magnesium, the basket was inverted and immersed in a salt-metal melt (90 mol % $CaCl_2$-10 mol % $CaF_2$/62 at. % Zn-32 at. % Mg-6 at. % Ca) contained in a second vessel. After the $UO_2$ pellets dropped out of the basket, the basket was removed and the melt was agitated to reduce the oxide pellets to metal. All operations for this experiment were performed remotely and were completed satisfactorily. Analytical data are not yet complete. The procedures followed were similar to the experimental procedures planned to be used with irradiated fuel.

C. Melt Decladding (I. O. Winsch, T. R. Johnson, T. F. Cannon, J. J. Stockbar)

The Fuel Cycle Branch of the RDT has asked ANL to evaluate melt decladding as a possible head-end process for discharged fast reactor fuels. In comparison with the shear-roast preparation for fuel dissolution, it appears that a melt-decladding head-end process requires fewer mechanical operations, provides some separation of the stainless steel from the fuel oxide prior to dissolution, produces more compact metallic waste, and facilitates collection of fission-product gas for storage. Approaches considered for separating molten stainless steel from fuel pellets are as follows:

1. Melting the steel and allowing it to solidify around the oxide, then separating the components by acid dissolution of the oxide. (This requires that no significant portion of the fuel becomes completely surrounded by stainless steel.)

2. Heating the fuel subassembly in a vertical crucible having holes in its base to allow drainage of the liquid stainless steel from $UO_2$ pellets and fines (ANL-7767, p. 19).

3. Melting the cladding while the fuel subassembly rests on a crucible wall sloped downward at a small angle to promote flow of molten metal away from the pellets (ANL-7767, pp. 19-22; ANL-7799, pp. 20-23).

4. Melting the stainless steel in an upright crucible and tipping the crucible to pour off the steel, having the oxide in the crucible.

5. Lowering vertically suspended fuel subassemblies slowly through an open-bottom furnace so that as the steel melts, the mixture of steel and fuel falls onto a cooled surface. The steel forms platelets that might be separable from the fuel (ANL-7799, p. 24).

1. Scouting Experiments

Results were reported in the previous report, ANL-7799, pp. 20-23, of a number of small-scale laboratory experiments using unirradiated assemblies of sintered $UO_2$ pellets contained in Type 304 stainless steel tubes. These experiments were intended to assist in preparing a rough evaluation of the process.

The final scouting experiments have now been completed. These experiments relate to the fifth approach listed above. It is expected that this procedure would allow some of the larger pieces of steel to be separated from the fuel oxide and would open the fuel pins to expose the oxide fuel for acid dissolution. Although it is anticipated that little separation of oxide and steel could be accomplished before the acid dissolution step, the steel would be solidified into compact shapes that could be more easily handled in the dissolver than the sections of tubing created by shearing. During lowering of the subassembly into the furnace, sodium and the fission gases in the gas plenum of the fuel pins would be separated from the fuel. Important advantages of this process concept over other melt-decladding concepts are that a simple furnace design would be used and there would be no requirement for a crucible capable of containing liquid steel.

Two experiments were made to simulate this process. An induction furnace was modified so that it had an open bottom permitting a 1 1/2-in. OD stainless steel tube to be lowered vertically into the heated zone. Drops of molten steel fell from that portion of the tube located in the hot zone, through a 6-in.-long unheated section of ceramic tube, and onto a cold steel tray inclined at a 45° angle.

In the first experiment, an empty stainless steel tube (1 1/2-in. OD, 1 1/4-in. ID, 4 1/2 in. long) was lowered into the hot zone. In the

second run, seven stainless steel tubes (0.25-in. OD, 0.23-in. ID) filled with 151 g of $UO_2$ pellets were supported in a stainless steel tube (4 1/2-in. long, 1 1/2-in. OD, 1 1/4-in. ID). In both experiments, the drops of molten steel initially formed thin plates with diameters of about 1 in.; these plates slid down the tray. When enough steel had collected in the tray to prevent the newly formed plates from sliding, the drops of metal collected in a mound under the hot zone. About 10% of the metal formed fines caused by splashing of the molten steel. During the second experiment, most of the $UO_2$ pellets fell with the first drops of metal. It was found that 80% of the oxide pellets were loose and that none of the pellets was wet by the steel. A few pieces of the 1/4-in. tube were found unmelted and a pellet was found in one of these tubes. All of the pellets had been exposed and could be dissolved by acid.

The metal shapes (the thin plates) formed in these experiments would not be significantly easier to handle than pieces of sheared tube bundles. However, it should be possible to devise a method to form a convenient shape from the steel. For example, the molten steel could be continuously cast into a thin strip which would then be cut into convenient lengths for feeding to an acid dissolver.

In another variation of the process, the drops of molten steel would fall into a liquid where they would solidify into spheres. Alkali nitrate salts are possible liquids that might be used for this purpose. Sodium salts that contain compounds such as NaOH, $Na_2CO_3$, or $NaNO_3$ oxidize $UO_2$ to form sodium uranates, which are insoluble in the liquid salt. The $PuO_2$ may not be oxidized, but the pellet would be disintegrated, releasing the volatile fission products. Following the release of volatile elements, the disintegrated fuel could be put into aqueous solution. A process employing nitrate salts to dissolve $UO_2$-Mo cermet fuel and to achieve a partial separation of uranium from molybdenum and fission products has been proposed by Bähr.[2]

## 2. Conceptual Design

A conceptual design is being prepared based on use of a tilt-pour melt-decladding furnace (Fig. I-1) capable of handling 1 metric ton of spent nuclear fuel per 8-hr day. In this concept, two vertically suspended fuel subassemblies in a cooled transport chamber are brought to the top of a furnace in a process cell. The transport chamber is fastened into position, and a lock is opened to allow the subassemblies to be lowered into a magnesia-lined graphite crucible, which is inductively heated. The rate of lowering is controlled to correspond to the rate at which the stainless steel melts. At the furnace temperature of 1550 to 1600°C, the stainless steel in the crucible is a liquid and the fuel oxide remains solid. After the melt-down period, about 1 hr, the crucible is tilted to about 10° below horizontal and the molten steel is poured into a waste-steel transport mold that has the capacity to contain the steel from 8 subassemblies (∿1 1/2 metric tons). At the end of a day, the transport mold is removed from the furnace through a lock. After the steel is poured, the crucible assembly is tilted 45° past horizontal in the opposite direction to dump the $UO_2$-$PuO_2$ pellets into a chute leading to a lock. The pellets then are carried in a transport vessel to a cooled storage area and subsequently fed to the $HNO_3$ dissolution step.

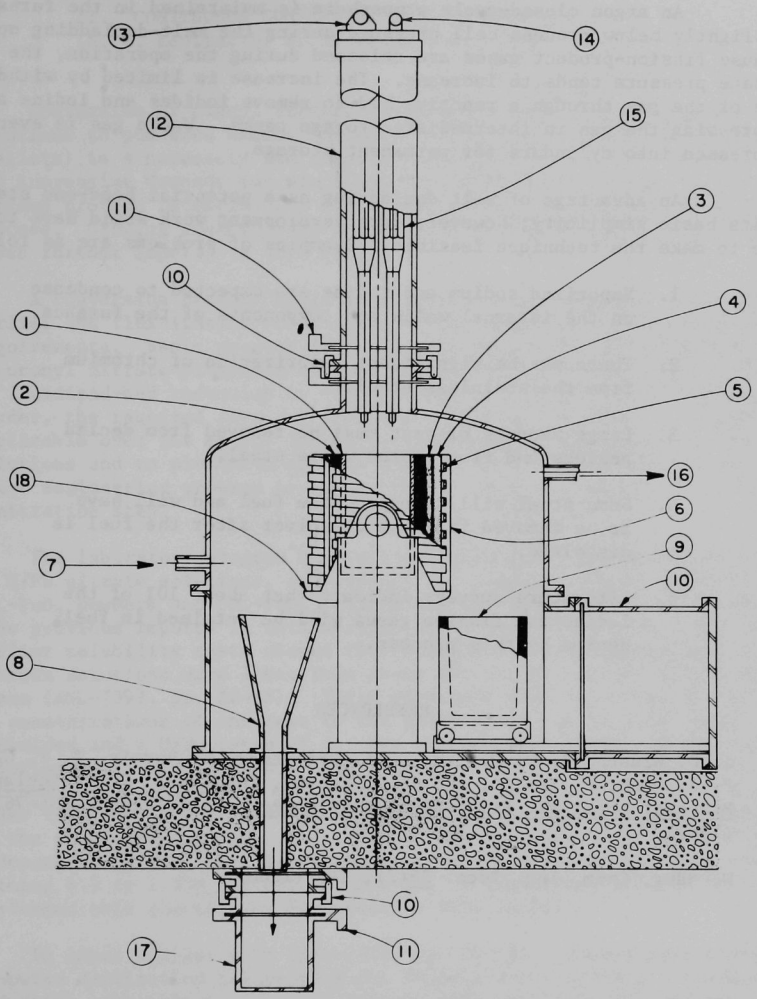


Fig. I-1. Tilt-Pour Melt Decladding Furnace. 1. MgO Liner of Crucible. 2. Graphite Crucible. 3. SiC Insulation. 4. Zirconia Insulation. 5. Induction Coils. 6. Coil Support. 7. Argon Supply. 8. $UO_2$-$PuO_2$ Fuel Chute. 9. Waste Steel Mold. 10. Locks. 11. Lock Gates. 12. Transfer Chamber. 13. Elevating Mechanism for Fuel Subassemblies. 14. Transfer Chamber Cooling Gas Inlet. 15. Fuel Subassemblies. 16. Argon + Fission Product Gas to Recycle and Storage. 17. Pellet Transport Vessel. 18. Tilt-Pour Mechanism for Crucible.

An argon closed-cycle atmosphere is maintained in the furnace at slightly below process cell pressure during the melt-decladding operation. Because fission-product gases are released during the operation, the furnace pressure tends to increase. The increase is limited by withdrawing some of the gas through a reactive bed to remove iodides and iodine and then compressing the gas in intermediate storage tanks. Waste gas is eventually compressed into cylinders for permanent storage.

An advantage of melt decladding as a potential head-end step is its basic simplicity; however, some development work would have to be done to make the technique feasible. Examples of problems are as follows:

1. Vaporized sodium and iodine are expected to condense on the internal walls and components of the furnace.

2. There may be significant vaporization of chromium from the stainless steel.

3. Large amounts of heat must be removed from declad pellets and from poured waste steel.

4. Some steel will accompany the fuel and will have to be removed from the dissolver after the fuel is dissolved.

5. Literature surveys indicate that about 10% of the iodine and fission gases will be retained in fuel declad by this process.

## REFERENCES

1. I. O. Winsch, R. D. Pierce, D. E. Grosvenor, L. Burris, T. F. Cannon, P. J. Mack, K. Nishio, and K. R. Tobias, The EBR-II Skull Reclamation Process: Part IV. Pilot-Plant Development, USAEC report ANL-7614 (1969).

2. W. Bähr, Chem. Ing. Tech. 38(2), 145 (1966).

## II. CONTINUOUS CONVERSION OF U/Pu NITRATES TO OXIDES
(N. M. Levitz, D. E. Grosvenor, S. Vogler, F. G. Teats)

Conversion of uranyl nitrate hexahydrate (UNH) and plutonium nitrate solutions to powdered oxides suitable for the fabrication of fuel shapes (pellets) is a necessary and important part of the nuclear fuel cycle. The increasing demands for plutonium for LMFBR and plutonium-recycle fuel systems provide incentive for developing a new high-capacity conversion process. Growing concern over shipment of plutonium as nitrate solution gives further impetus to this effort.

A conversion process based on fluidized-bed technology developed in earlier ANL fluidization work[1] shows a high potential for meeting process requirements. Basic process steps include fluidized-bed codenitration of uranyl nitrate-plutonium nitrate solutions to $UO_3$-$PuO_2$ powder, followed by fluidized-bed reduction of the $UO_3$-$PuO_2$ with hydrogen to $UO_2$-$PuO_2$ powder, the required form for fuel manufacture. The process appears to be applicable over the entire concentration range of uranium-plutonium nitrate solutions and to plutonium nitrate alone. An integrated laboratory and pilot engineering program is in progress. Initial emphasis is on the denitration step.

The laboratory program has included solubility and stability studies on U/Pu nitrate solutions, and exploratory preparations of $UO_3$-$PuO_2$ and $UO_2$-$PuO_2$ powders and $UO_2$-$PuO_2$ pellets for preliminary characterization (see previous reports in this series, ANL-7735, -7755, -7767, and -7799). Earlier solubility tests showed that crystallization temperatures of U/Pu nitrate solutions were lower than those for uranyl nitrate solutions alone (ANL-7799, pp. 28-35). Tests were made with solutions in the range of concentrations of interest to the pilot plant, up to 2.0M total actinides and a U/Pu ratio of 4. Use of such relatively concentrated feed solutions will be practical. The change in valence distribution of plutonium (VI) and (IV) ions in nitrate solution was found to be a zero-order reaction with respect to Pu(VI) for a 50-day period (ANL-7755, p. 38); in the same investigation, the rate of valence change was observed to be independent of the initial plutonium concentration for solutions containing 0.3 to 1.35M plutonium. Results of additional solubility tests performed this quarter are discussed in this report.

In other earlier work (ANL-7799, pp. 25-29), powders were prepared by dropwise denitration (simulating the fluidized-bed process), followed by reduction with hydrogen. A few pellets were made from the reduced material. Examination of each of the materials by electron-microprobe techniques showed good distribution of the $PuO_2$ fraction ($\sim$0.2) in both the $UO_3$ and $UO_2$ matrixes. Pellet densities up to 89% of theoretical were achieved in the exploratory pressing and sintering tests. Characterization studies will be resumed when materials prepared in the pilot plant become available.

The pilot plant comprises a 4-in. dia fluidized-bed reactor and associated equipment. The equipment was installed in a glovebox and given preliminary shakedown tests with uranyl nitrate feed solutions (ANL-7755, pp. 40-44). During this report period, modifications of the denitration pilot plant were completed to satisfy the general safety and criticality

safety requirements for a plutonium facility and testing of the equipment was resumed.

## A. Laboratory Program - Solubility Studies on U/Pu Nitrate Solutions

A knowledge of the cosolubility of uranyl nitrate and plutonium nitrate in dilute nitric acid is important to the selection of the feed composition for the fluid-bed denitration pilot plant. Earlier tests (ANL-7799) were made on freshly prepared solutions, which contain a relatively high proportion of Pu(VI) as well as Pu(IV). On standing, hexavalent plutonium is reduced to the tetravalent state by alpha radiation (see ANL-7755), and it is of interest to determine whether the plutonium valence state affects the crystallization temperature. Crystallization experiments on solutions that had been stored for three months were carried out this quarter. Essentially the same crystallization temperatures were obtained as for freshly prepared solutions, showing that the plutonium valence state has little if any effect on crystallization temperature.

Two additional crystallization experiments were carried out to confirm and extend the earlier results. The solutions contained a greater plutonium fraction than in the earlier experiments; also, the plutonium was present as the tetravalent ion. The test solutions contained 1.4M total heavy metal ions and 3.4M nitric acid; the percentage plutonium in one solution was 50% and in the other 66.7%. The measured temperatures of crystallization were -1.7 and -8.5°C, respectively. A plot of these new data along with the earlier results is given in Fig. II-1. Relatively high stability of plutonium nitrate is achieved in these solutions, probably as a consequence of stable complex ions formed between plutonium (IV) ions and nitrate ions in nitric acid solutions.

The new data also confirm that the invariant point in the uranium-plutonium-nitric acid system lies on the plutonium-rich side, beyond 67% plutonium. Until the invariant point is reached, uranyl nitrate will be the precipitating species. This is important for criticality safety. We will use uranyl nitrate-20% plutonium nitrate solutions as the basic feed solution for our process work.

### 1. Identification of Crystalline Phase

Because of the importance of ensuring that plutonium does not crystallize from solution, several experiments were carried out to identify the crystallized phase at solution concentrations of process interest. The procedure consisted of crystallizing a fraction of the material from solution and separating the precipitate from the bulk of the solution by centrifuging and decanting. The crystallized material was dissolved in 1M nitric acid, and the solution was analyzed for plutonium by alpha liquid scintillation counting. The uranium-to-plutonium ratio was determined by X-ray fluorescence analysis.

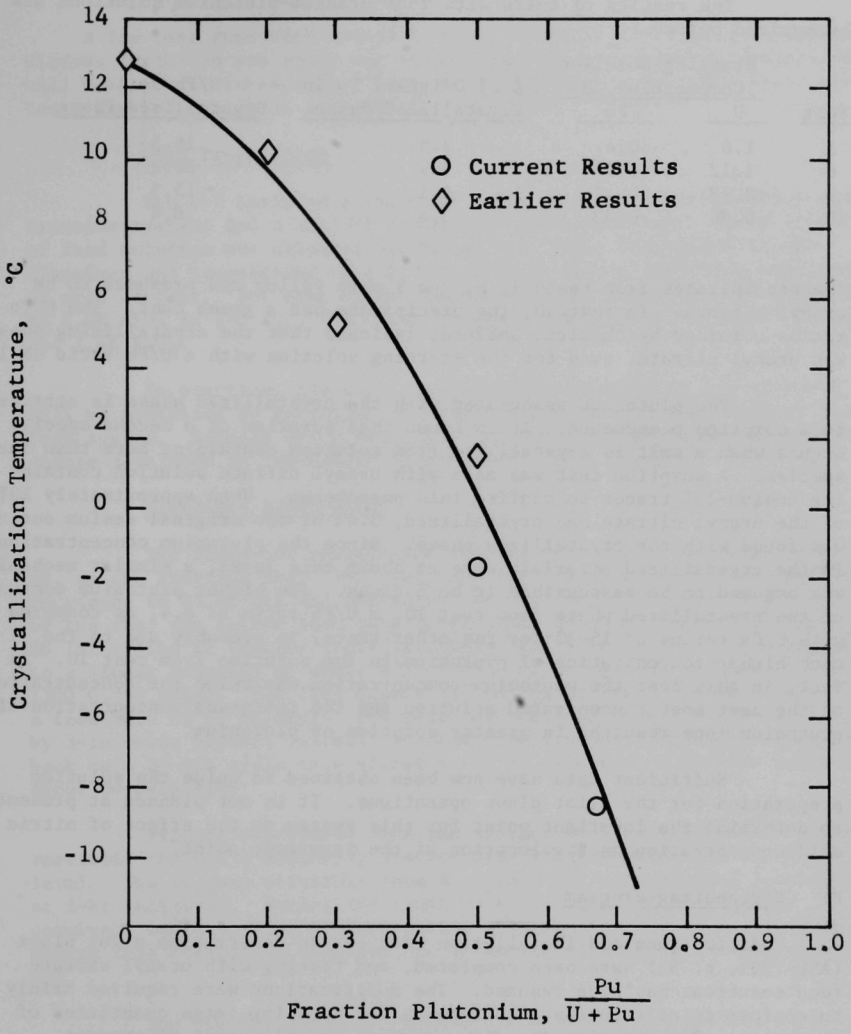


Fig. II-1. Crystallization Temperature of 1.4M (U,Pu) Nitrate Solutions as a Function of Plutonium Concentration

$HNO_3$ Content: 3.4M

2. Results

The results of tests with four uranium-plutonium solutions are summarized below:

| Test | Starting Solution Composition, M U | Pu | % of Original Pu in Crystallized Phase | U/Pu Ratio, Crystallized Phase |
|---|---|---|---|---|
| 1 | 1.6 | 0.4 | 2.5 | 16.5 |
| 6 | 1.12 | 0.28 | 3.9 | 20.2 |
| 9 | 0.98 | 0.42 | 2.1 | 15.5 |
| 10 | 0.86 | 0.82 | 3.4 | 8.4 |

The precipitates from tests 1, 6, and 9 were yellow and presumed to be uranyl nitrate. In test 10, the precipitate had a green cast. The U/Pu ratios obtained by chemical analyses indicate that the crystallizing phase was uranyl nitrate, even for the starting solution with a U/Pu ratio of 1.

The plutonium associated with the crystallized phase is attributed to a sorption phenomenon. It is known that sorption of a second species occurs when a salt is crystallized from solution containing more than one species. A sorption test was made with uranyl nitrate solution containing cesium-137 tracer to confirm this phenomenon. When approximately 10% of the uranyl nitrate had crystallized, 3.4% of the original cesium activity was found with the crystallized phase. Since the plutonium concentrations in the crystallized materials were at about this level, a similar mechanism was assumed to be responsible in both cases. The higher plutonium content of the crystallized phase from test 10, a U/Pu ratio of 8.4, as compared with U/Pu ratios of 15-20 for the other tests, is probably due to the much higher concentration of plutonium in the solution from test 10. In fact, in this test the plutonium concentration was twice the concentration of the next most concentrated solution and the increased concentration of plutonium ions resulted in greater sorption of plutonium.

Sufficient data have now been obtained to guide the solution preparation for the pilot plant operations. It is not planned at present to determine the invariant point for this system or the effect of nitric acid concentration on the location of the invariant point.

B. Engineering Program

Modifications and installation work on the denitration pilot plant (ANL-7735, p. 54) have been completed, and testing with uranyl nitrate feed solutions has been resumed. The modifications were required mainly to conform to criticality requirements for handling large quantities of plutonium. For example, the size, number, and placement of product receivers were fixed, and vessels larger than 4 in. in diameter were filled with boron-glass Raschig rings as a fixed nuclear poison. Modifications were also made to the feed system. The feed system was redesigned to consist of three vessels: a dissolver (4-in. dia by 36 in. tall), a feed storage vessel (16-in. dia by 25 in. tall and filled with boron-glass Raschig rings), and a feed metering tank (3-in. dia by 40 in. tall) from which the solution is metered to the fluidized-bed reactor. Two pumps

are employed, one for intervessel transfer and the second as the feed metering pump.

A few test runs with uranyl nitrate solutions and with the glovebox windows installed are under way to evaluate equipment and procedures that will be used for subsequent studies with U/Pu solutions. The first such test, Run U-7, has been successfully completed.

1. Feed Preparation

Run U-7 included a thorough check of the feed preparation and transfer systems and a 10.5-hr fluid-bed denitration run. Fifty liters of feed solution was prepared batchwise in 5-liter increments in the dissolver and transferred to the feed storage vessel for final adjustment of acid content. For each batch dissolution, 3.2 kg of $UO_3$ was dissolved in 6.0M $HNO_3$ in 1-2 hr. The final solution contained 1.9M uranyl nitrate and 1.4M $HNO_3$.

In practice, the total quantity of plutonium in the glovebox will be minimized by recycling $UO_3$-$PuO_2$ denitration product back to the feed system. Batches of $UO_3$-$PuO_2$ will be dissolved according to a procedure developed in laboratory studies (ANL-7735, p. 49).

2. Fluid-Bed Denitration

The fluid-bed denitration run was made at 300°C, using 10 kg of $UO_3$ as the starting bed. The feed rate was initially 65 ml/min, but was increased to 95 ml/min and maintained at that rate for about the last 7 hr of the run; the latter feed rate corresponds to a $UO_3$ production rate of 80 lb/(hr)(sq ft reactor cross section). The inlet gas flow corresponded to a linear velocity of about 0.9 ft/sec, calculated at column conditions (300°C, ∿5 psig). The feed nozzle air-to-liquid ratio was 420 (based on a feed rate of 95 ml/min). The sintered metal filters (two 18-in.-long by 3-in.-wide bayonet filters) mounted directly above the bed were blown back on a 20-min cycle (one filter every 10 min) with a 0.1-sec pulse of about 80-psig air.

Product overflowed from the reactor continuously into a collection reservoir through a nominally 1/4-in. pipe sidearm welded at the 12-in. level. The $UO_3$ was withdrawn from the reservoir into product receivers at 1-hr intervals. During the final 2 hr, plugging of the sidearm occurred, necessitating product removal through the bottom drain valve during this period. A constant bed level was maintained for the entire run.

The run was evaluated mainly on the basis of particle size distribution of the product. A sample splitter was used to obtain small (25- to 40-g) representative samples from the starting and final beds and samples taken at hourly intervals. Particle size distribution was determined using an Allen-Bradley Sonic Sifter.

The results of the sieve analysis of the $UO_3$ product are presented in Table II-1. The apparent increase in average particle size from 200 μm to 234 μm between the starting bed and the sample taken after the first

TABLE II-1. Sieve Analysis of $UO_3$ Product from Denitration Run U-7

| Hourly Sample Number | wt % of sample on given sieve | | | | | | | Mean Particle Dia, μm |
|---|---|---|---|---|---|---|---|---|
| | +20 | -20+40 | -40+60 | -60+100 | -100+200 | -200+325 | -325 | |
| 0[a] | 1.1 | 7.8 | 48.6 | 29.0 | 8.8 | 3.9 | 0.7 | 200 |
| 1 | 2.8 | 10.2 | 49.4 | 27.3 | 8.5 | 1.7 | 0 | 234 |
| 2 | 3.6 | 17.6 | 49.5 | 25.1 | 4.3 | 0 | 0 | 279 |
| 3 | 5.9 | 19.6 | 46.1 | 27.4 | 1.5 | 0 | 0 | 302 |
| 4 | 5.0 | 18.9 | 43.5 | 29.0 | 3.1 | 0.3 | 0 | 279 |
| 5 | 3.3 | 16.9 | 43.1 | 32.5 | 3.9 | 0.3 | 0 | 264 |
| 6 | 3.4 | 15.3 | 43.2 | 33.4 | 4.7 | 0 | 0 | 262 |
| 7 | 3.7 | 14.7 | 43.1 | 33.1 | 5.3 | 0 | 0 | 259 |
| 8 | 2.0 | 12.0 | 43.0 | 36.1 | 6.4 | 0.4 | 0 | 241 |
| 9 | 0.3 | 7.2 | 42.8 | 42.8 | 6.7 | 0.3 | 0 | 229 |
| 10[b] | 1.8 | 13.0 | 40.3 | 36.6 | 7.5 | 0.7 | 0 | 236 |

[a] Starting bed, average of two samples.

[b] Final bed data, corrected for >10 mesh fraction; mean particle diameter was calculated only for the <10 mesh fraction.

hour merely reflects the loss (elutriation) of fines (-200 mesh) from the bed. The remaining sieve analyses show that a low level of fines was present in the bed throughout the run. After the bed was removed, approximately 200 g of fines was recovered from the reactor by rapping on the column. Overall, the fines inventory in the bed remained fairly uniform.

Sieve analyses show that the average particle size peaked at about 3 hr and then gradually diminished, but no conclusions regarding size distribution trends can be drawn in view of the short duration of the run.

Approximately 2.8% of the $UO_3$ particles produced were greater than 10 mesh; some of the particles, obviously nozzle growths, were as large as 1 in. across. All coarse material was removed with the final bed; material larger than 10 mesh represented about 7% of the final bed weight. Accumulation of coarse material in the bed did not interfere with operation of the reactor.

One or two additional runs with uranyl nitrate feed solution are planned. Other remaining work includes testing of the glovebox for leaks and a test of the efficiency of the AEC filters installed in the glovebox. Work with plutonium solutions will then begin.

## REFERENCE

1. A. A. Jonke, E. J. Petkus, J. W. Loeding, and S. Lawroski, Nucl. Sci. Eng. 2, 303 (1957).

## III. IN-LINE ANALYSIS IN FUEL FABRICATION
(J. G. Schnizlein, T. Gerding, M. J. Steindler)

The economic competitiveness of the LMFBR can be improved by lowering the fuel fabrication costs. The development of rapid, precise, and accurate in-line nondestructive methods for the analysis of critical fuel properties for the large number of fuel pellets that will be processed can help to significantly decrease these costs and lead to automated procedures. The starting criteria that we have selected for evaluation of analytical requirements are the specifications (and associated precision) for preirradiation fuel properties for the Fast Fuel Test Facility (FFTF) project.

The fuel properties, specifications, precisions, and acceptable methods of measurement for FFTF were discussed in an earlier quarterly report (ANL-7735, pp. 60, 63-64). Recent standards and specifications[1] have relaxed some of the criteria for acceptable properties. Possibly, as additional information on fuel performance is obtained from irradiation experiment, specifications for fuel properties will become less rigorous.

The fuel for the first commercial LMFBRs is expected to be uranium-plutonium oxide. The properties selected for initial study are the plutonium/uranium (Pu/U) ratio and oxygen/metal (O/M) ratio, which properties will be evaluated in any conceivable fabrication procedure. A literature survey indicating that the O/M ratio can be determined with adequate precision by measurement of lattice parameters of the fuel oxide is described in ANL-7735, pp. 65, 71-80.

### A. Plutonium/Uranium Ratio in Fuel

X-ray fluorescence (XRF) analysis is being evaluated as a nondestructive, in-line analytical method for determining Pu/U ratios in fuel materials. In XRF, the characteristic radiation of the element is excited by incident X-rays of energy higher than the absorption edge.

The originally defined specification for plutonium content in the fuel (ANL-7735) required a core zone to have a plutonium content of $20.0 \pm 0.1\%$, which imposed a relative precision of 0.5% on the analysis. The recently relaxed specification which requires a relative precision of 1% offers greater opportunity for rapid and automated analytical procedures. To attain the desired relative precision in the analysis of solid oxide in the form of powder or pellets, effects on the fluorescence signal of properties of the solid, i.e., high absorption coefficients, enhancement (secondary fluroescence), crystallite size, bulk density, etc., must be proved insignificant or predictably measurable. Absorption losses are a result of scattering from the surface by voids and by grains, as well as absorption by other elements present. The XRF method, utilizing the $L\alpha$ spectra, has been shown to be free of interferences by any other elements that can reasonably be expected to be present in a fuel sample (ANL-7799, pp. 36-41).

$ThO_2$-$UO_2$ is being used as a stand-in for $UO_2$-$PuO_2$ for initial investigations to avoid the complications and delays of experiments with

plutonium, which would have to be done in a glovebox. This substitution is practical because of the identical relationship of the atomic numbers of each pair of elements and thus of the relevant properties (see ANL-7755, pp. 45-46). For example, enhancement or secondary fluorescence occurs in both pairs because the characteristic radiation from one element in each pair has enough energy to excite the characteristic radiation of the other element of the pair. In uranium-plutonium oxides, PuL$\beta$ excites UL$\alpha$, and in thorium-uranium oxides, UL$\beta$ excites ThL$\alpha$.

In the experimental program to demonstrate the practicality of this analytical method, instrumental choices, sample presentation procedures, and material effects are being evaluated. Consideration of a desirable sampling procedure to accommodate a high production rate of fuel and to extend the ultimate limitation imposed by counting statistics led to the use of wider collimating slits to decrease the analysis time per sample to less than one minute. With a slit width of 20 mils, adequate resolution of the pairs of peaks to be counted was demonstrated (ANL-7755, pp. 45-50). Improvements in the sample presentation procedure (ANL-7767, pp. 30-31) increased the counting rate and decreased the background. The counting equipment has been calibrated for high count rates to account for dead time and coincidence (ANL-7799).

1. Analysis of Pellets

An investigation is under way to determine whether a relative standard deviation of $\pm$0.5% at the 95% confidence level can be achieved for plutonium analysis of mixed-oxide fuel materials.

Materials examined included four pellets of each of the concentrations, 10, 20, and 30 wt % $UO_2$ in $ThO_2$, prepared from the mixed powders. Four $UO_2$ pellets were prepared from pure $UO_2$ powder. The pellets were sintered in a 6% $H_2$-He atmosphere at 1750°C for 4 hr, and the flat surfaces were polished with 600-grit paper.

In order to determine the functional reproducibility of the X-ray fluorescence measurements on pellets, a series of five measurements was performed on each pellet of each composition. An example of the data is shown in Table III-1, which illustrates the results for thorium and uranium measurements of $ThO_2$-30 wt % $UO_2$ pellets. The average count rate and relative sigma for the five measurements on each pellet are at the right of the table. Each count rate within the matrix was an average of three counts of $\sim$200,000 each, giving $\sigma_{count}$ = 0.11%. Each count rate was corrected for dead time (coincidence).

An analysis of variance[3] was performed to compare the variability of measurements on the same pellet (ascribed to variability of the method) with the variability of measurements of different pellets of the same nominal composition. The calculation for uranium in the $ThO_2$-30 wt % $UO_2$ pellets is presented in Table III-2. If it is assumed that the errors of the method and counting statistics are independent and that therefore the variances are additive, the relative standard deviation (RSD) of the method can be calculated from the variance of the measurements and the variance of the counting statistics. Table III-3 presents the relative standard deviations for measurements, for counting statistics, for errors of the

TABLE III-1. Results of XRF Measurements of Thorium and Uranium in a Series of $ThO_2$-30 wt % $UO_2$ Pellets

X-ray generator settings: 50 kVp, 35 mA, Sn Filter

| Pellet | ULα Measurement, cps[a] 1 | 2 | 3 | 4 | 5 | Average | $\sigma_{rel}$,% |
|---|---|---|---|---|---|---|---|
| 1 | 15344 | 15257 | 15316 | 15284 | 15343 | 15309 | 0.22 |
| 2 | 15448 | 15441 | 15469 | 15459 | 15421 | 15448 | 0.11 |
| 3 | 15303 | 15289 | 15278 | 15306 | 15315 | 15298 | 0.088 |
| 4 | 15294 | 15273 | 15285 | 15288 | 15307 | 15289 | 0.073 |
| | | | | | Grand Mean[b] | = 15336 | |
| | | | | | $\sigma_{rel}$,% | = 0.46% | |

| Pellet | ThLα Measurement, cps[a] 1 | 2 | 3 | 4 | 5 | Average | $\sigma_{rel}$,% |
|---|---|---|---|---|---|---|---|
| 1 | 31932 | 31828 | 31924 | 31858 | 31901 | 31889 | 0.12 |
| 2 | 31981 | 32116 | 31952 | 32043 | 32034 | 32025 | 0.18 |
| 3 | 31931 | 31834 | 31691 | 31953 | 31801 | 31842 | 0.30 |
| 4 | 31921 | 31837 | 32017 | 31972 | 32010 | 31951 | 0.21 |
| | | | | | Grand Mean[b] | = 31927 | |
| | | | | | $\sigma_{rel}$,% | = 0.31 | |

[a] Each count rate in the table is an average of three counts of ∿200,000, and each is corrected for dead time; $\sigma_{count}$ = 0.11%.

[b] Grand mean = average of the averages.

TABLE III-2. Analysis of Variance for

X-ray Fluorescence Measurement of Uranium in $ThO_2$-30 wt % $UO_2$[a,b]

| Source | Sum of Squares | Degrees of Freedom | Mean Square | Quantity Estimated by Mean Squares |
|---|---|---|---|---|
| Between pellets | $S_1 = 84126$ | 3 | $M_1 = 28042$ | $\sigma_o^2 + n\,\sigma_1^2$ |
| Within a pellet | $S_0 = 8618.0$ | 16 | $M_0 = 538.6$ | $\sigma_o^2$ |
| Total | 92744 | 19 | 4881.2 | |

[a] See Ref. 3, Ch. 6.

[b] $\sigma_o^2 = \sigma^2_{\text{measurement}}$ and $\sigma_1^2 = \sigma^2_{\text{pellet}}$ of Table III-3.

n = number of measurements of each pellet = 5, number of pellets = 4

TABLE III-3. Relative Standard Deviations for XRF Analysis of Fired $ThO_2$-$UO_2$ Pellets

| $ThO_2$, wt % | $UO_2$, wt % | $\sigma_{measurement}$,[a] % (within pellets) | $\sigma_{count}$,[b] % | $\sigma_{method}$,[c] % | $\sigma_{pellet}$,[d] % (between pellets) |
|---|---|---|---|---|---|
| | | | Uranium Analyses | | |
| 0 | 100 | 0.14 | 0.086 | 0.11 | e |
| 70 | 30 | 0.15 | 0.11 | 0.10 | 0.62 |
| 80 | 20 | 0.34 | 0.13 | 0.31 | 1.84 |
| 90 | 10 | 0.33 | 0.13 | 0.30 | 0.87 |
| | | | Thorium Analyses | | |
| 70 | 30 | 0.27 | 0.11 | 0.24 | e |
| 80 | 20 | 0.27 | 0.10 | 0.24 | 1.12 |
| 90 | 10 | 0.26 | 0.099 | 0.24 | 0.60 |

[a] RSD derived from five measurements on same pellet.

[b] RSD derived from three counts corrected for dead time (see Table III-1, footnote a).

[c] RSD derived from the square root of the quantity, $\sigma^2_{measurement} - \sigma^2_{count}$.

[d] RSD for four different pellets having the same nominal composition.

[e] Null hypothesis (F test) indicates that the variability between pellets did not differ significantly from the variability within pellets.

method, and for the variability between pellets, derived from both uranium and thorium XRF count rates.

As expected, for the pure urania pellets, the variability between pellets is not statistically different from the variability within pellets. The RSD for the method applied to pure $UO_2$ pellets, considering the RSD for counting statistics and the RSD for measurements, is 0.11%.

For the $ThO_2$-30 wt % $UO_2$ pellets, the thorium analyses show that the variability between pellets is not statistically different from that within pellets; however, uranium analyses for $ThO_2$-30 wt % $UO_2$ pellets show that variability between pellets is significant.

For the $ThO_2$-20 wt % $UO_2$ and $ThO_2$-10 wt % $UO_2$ pellets, the RSD for measurements for both $UO_2$ and $ThO_2$ leads to a range of RSD of the method of 0.24 to 0.31%. The 95% confidence limits of the RSD can be estimated by using the appropriate degrees of freedom in reference tables.* The largest upper limit calculated at the 95% confidence level of the RSD of measurements is 0.48%. Thus, the XRF method applied to pellets appears capable of achieving the goal of 0.5% relative standard deviation at the 95% confidence level.

A range of 0.60 to 1.84 for RSDs between mixed-oxide pellets was calculated from uranium and thorium analyses, indicating variation in excess of that attributable to the method. The excess variability may be due to mixing, blending, sampling or material properties of mixtures.

2. Uranium Content of $ThO_2$-$UO_2$ Mixed Powder

The intensities of the Lα emission lines from uranium and thorium were measured for powder mixtures of $ThO_2$-30 wt % $UO_2$. The mixtures were prepared from pure $ThO_2$ and from $UO_2$ that had been reduced from NBS $U_3O_8$.

An analysis of variance similar to that for pellets was performed for $ThO_2$-30 wt % $UO_2$ powder by performing five measurements on each of three powder samples. Three sample cups (ANL-7767) were loaded with powder and were counted sequentially for five measurements on each. The RSDs for the measurements were 0.29% for thorium and 0.21% for uranium, which lead to RSDs for the method of 0.27% and 0.17%, respectively, at the 95% confidence level, again below 0.5%.

No significant variability between samples of powder was indicated by the thorium analyses; the uranium analyses showed a RSD of 3.1%. This greater variability between samples of powder (3.1%) than between pellets (0.62%) of the same nominal composition suggests a material effect in powder that is greater than in pellets.

---

*Five measurements on four samples gives 16 degrees of freedom. The nearest degree of freedom in Table H of Davies (p. 107) is 15, leading to factors of 0.75 and 1.55 for 95% confidence limits.

It is still to be determined whether variations in powder properties allow attainment of the necessary precision and accuracy. Normally, quantitative analysis by a fluorescence technique requires a set of standards covering the range of variables of interest, such as composition (element concentration and matrix content), density, grain size, and absorption coefficients. Criss and Birks[2] have formulated methods whereby X-ray fluorescence can be calculated from fundamental parameters. Computer calculations could greatly decrease the number of standards necessary by allowing some prediction of signal losses due to material properties. Nevertheless, experimental work will be required to verify the effect of certain variables on fluorescence intensity. Studies of the effects of particle size and bulk density on the XRF signal are expected to identify the limiting precision of the method applied to powder samples.

## 3. Conclusions

The adequately low variability of the method indicates that XRF has the potential to achieve better than 0.5% RSD at 95% confidence level. The larger variability between samples of powder and pellets compared with the variability of the method indicates that a problem exists due to mixing, blending, sampling, or material properties. By study of particle size and bulk density effects on the XRF signal using pure materials and mixtures, it is expected that the precision obtainable for powder mixtures as well as the feasibility of improving this precision by pelleting will be evaluated.

## REFERENCES

1. RDT Standard, FFTF Driver Fuel Pin Fuel Pellet, RDT E 13-6, Oct. 1970.

2. J. W. Criss and L. S. Birks, Anal. Chem. 40, 1080 (1968).

3. O. L. Davies (ed.), Statistical Methods in Research and Production, 3rd Ed., Hafner Publishing Co., New York (1961).

# IV. ADAPTATION OF CENTRIFUGAL CONTACTORS IN LMFBR FUEL PROCESSING

(G. Bernstein, J. Lenc, N. Quattropani)

Performance characteristics of a centrifugal contactor suitable for use during plutonium purification (plutonium-isolation steps) in Purex-type solvent extraction of LMFBR fuel material are being investigated. The contactor (ANL-7799, pp. 43-45) is a modification of the large centrifugal contactors in use at the Savannah River plant. In the ANL design, criticality hazards caused by the high plutonium concentrations in the process streams will be controlled by limiting the diameter to a geometrically favorable dimension. Expected advantages of centrifugal contactors are (1) reduced radiation damage to the solvent as a result of brief residence time in the contactor and (2) improved ease of operation (including rapid flushout at the end of a processing campaign).

Additional tests were made to evaluate the hydraulic and mechanical performance of the stainless steel centrifugal contactor, which has a hollow rotor with a 4-in. ID and a 15-in. length (including a 12-in. long settling zone). Separating capacity* was measured over a range of rotor speeds of 2000 to 3500 rpm and aqueous-to-organic (A/O) flow ratios of 0.33 to 4.0. The aqueous phase was 0.5M $HNO_3$. The organic phase was either 15 or 30% tributyl phosphate (TBP) in Ultrasene (refined kerosene).

In the experiments with 15% TBP at A/O ratios of ∿2.0, separating capacity was near the minimum value at all rotor speeds tested. At A/O ratios above and below ∿2.0, separating capacities were higher. At all A/O ratios, capacity increased with increasing rotor speed. As shown in Fig. IV-1, capacities at A/O = 0.5 ranged from about 6.8 gpm at 2000 rpm to about 11.4 gpm at 3500 rpm. At A/O = 3, capacity was 9.2 gpm at 2000 rpm. At rotor speeds above 2000 rpm, throughput was found to be limited by the size of the inlet piping. The piping was subsequently enlarged for the tests with 30% TBP.

In the tests with 30% TBP, minimum separating capacity over the range of speeds from 2000 to 3500 rpm was found at an A/O ratio of ∿1.0. The larger inlet lines permitted higher flow rates than had been attainable when 15% TBP in Ultrasene was used. Accordingly, capacities as high as 17 gpm were attained at a rotor speed of 3500 rpm and an A/O ratio of 4. As shown in Fig. IV-2, the relative increase in capacity at low A/O ratios was less than had been achieved with 15% TBP in Ultrasene (Fig. IV-1).

During these tests, the air-controlled aqueous weir (ANL-7799, p. 47) performed satisfactorily in positioning the aqueous-organic emulsion (or interface) band between the organic and aqueous weirs at the top of the

---

*Separating capacity is arbitrarily defined as the maximum total flow throughput with no more than 1 vol % entrainment of either phase in the exit stream of the other phase.

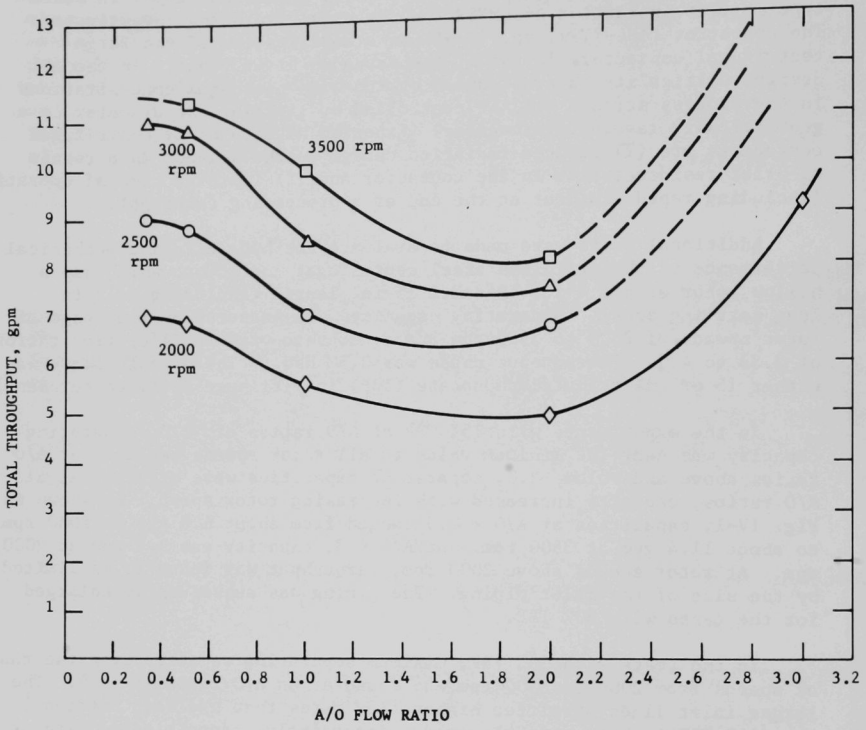


Fig. IV-1. Separating Capacity of 4 in. dia Rotor Centrifugal Contactor

Aq. - 0.5M $HNO_3$

Org. - 15% TBP in Ultrasene

<1% entrainment

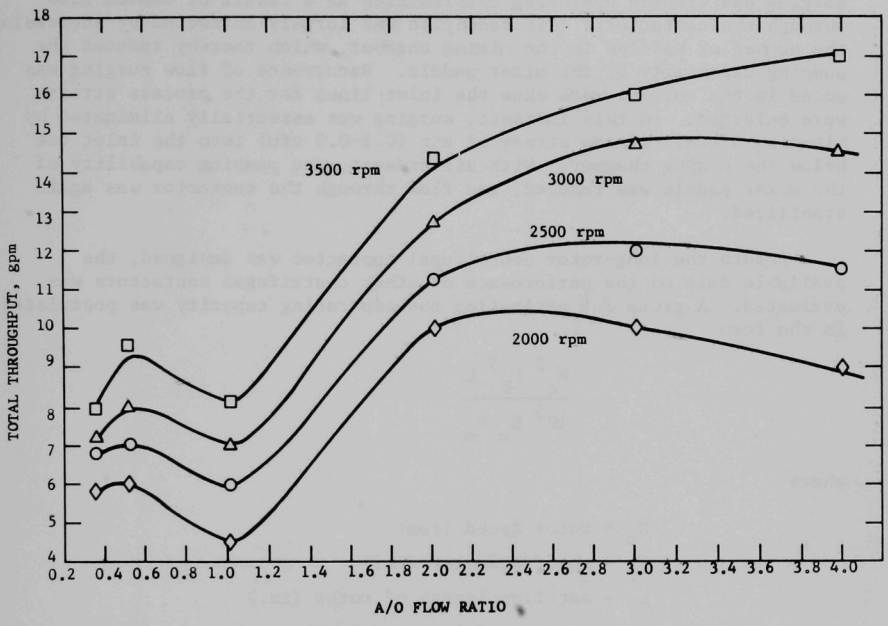


Fig. IV-2. Separating Capacity of 4-in. dia Rotor Centrifugal Contactor

Aq. - 0.5M $HNO_3$

Org. - 30% TBP in Ultrasene

<1% entrainment

rotor (where the aqueous and organic phases are separated). Air pressures required to achieve desired interface control ranged from 0 to 4 psi and conformed closely to the values calculated on the basis of formulas developed at Savannah River.[1]

The preceding report in this series (ANL-7799) stated that flow surging had created operating difficulties as a result of uneven flow through the contactor. This condition was largely corrected by increasing the number of baffles in the mixing chamber, which thereby reduced the pumping capability of the mixer paddle. Recurrence of flow surging was noted in the current work when the inlet lines for the process streams were enlarged. In this instance, surging was essentially eliminated by bleeding a small steady stream of air (0.2-0.3 cfm) into the inlet tee below the mixing chamber. With air present, the pumping capability of the mixer paddle was reduced, and flow through the contactor was again stabilized.

Before the long-rotor centrifugal contactor was designed, the available data on the performance of other centrifugal contactors was evaluated. A group for estimating the separating capacity was postulated in the form

$$\frac{N_c^{\,2} D_b^{\,3} L}{10^5 N_m D_m}$$

where

$N_c$ = rotor speed (rpm)

$D_b$ = rotor diameter (in.)

$L$ = settling length of rotor (in.)

$N_m$ = mixing paddle speed (rpm)

$D_m$ = paddle diameter (in.)

The numerical value of the group is divided by a conversion factor of $10^5$ to give an approximate capacity in gpm. On the basis of rotor speed, diameter, and settling zone length of the ANL contactor, a separating capacity of about 10 gpm at 3500 rpm was predicted. The capacity was expected to be within a factor of two of this value, varying with solution composition and A/O flow ratio. In the tests with the ANL contactor, capacity at 3500 rpm ranged from 8 to 17 gpm. These values are in good agreement with the predicted capacity and indicate that the relationship used in the calculation is valid.

Performance of the unit, to date, demonstrates that small-diameter long-rotor contactors can be operated stably at high speed and have high capacity. Factors related to critical speed and dynamic balance have to be carefully considered in the design of such units.

## REFERENCE

1. A. A. Kishbaugh, Performance of a Multi-stage Centrifugal Contactor, USAEC report DP-841 (Oct. 1963).

# V. THE ELECTROLYTIC REDUCTION AND REOXIDATION OF PLUTONIUM IN PUREX PROCESSES

(W. J. Mecham)

Adjustment of plutonium valence between +3 and +4 in high-plutonium solutions by an on-stream electrolytic method is being investigated, primarily for application to the plutonium isolation steps of the Purex process (ANL-7799, pp. 48-49). Changing the valence state of plutonium during solvent extraction allows its separation from fission-product contaminants. Electrolytic reduction, which would be a substitute for currently used chemical methods, would have the advantages of process stability, safety, and economy, as well as avoiding the storage of waste from chemical reductants, which in Purex processes are mixed with highly radioactive wastes. The work here reported is part of a program of development studies for assuring the capability of Purex technology for reprocessing LMFBR fuel.

In the preceding quarterly report in this series (ANL-7799), Krumpelt presented an introductory analysis of the electrochemistry and the process application. The principal variables were identified, and their interaction was discussed in some detail with regard to the most promising line of design and development for a cell having short residence time, low pressure drop, and adequate conversion efficiency for a favorable process application.

Currently, engineering design studies are under way, including (a) the development of engineering data from laboratory results and other sources, (b) the generation, analysis, and evaluation of alternative electrolytic cell designs, and (c) the specification, on the basis of design analyses and tests, of an electrolytic cell design suitable for plant application. This cell design would have to be verified and optimized by subsequent experimental studies of a prototype engineering-scale electrolytic cell.

In this report, the engineering basis of cell design is emphasized. The principles of cell design are developed with reference to the state of the art and in the form of calculational models which could be a basis for optimization of cell design. Two cell designs are presented illustrative of reference designs which might be evaluated by component testing and process demonstration.

## A. Design Parameters: Analysis of Experimental Performance of Flow Electrolyzers for Reduction of Uranium

The conceptual cell design (ANL-7799, pp. 60-65) consists of an anode and a cathode in individual compartments, separated by a diaphragm. The diaphragm (discussed in Section B.4 below) is permeable to ions, allowing ionic conduction of cell current, but prevents mixing of the bulk liquids of the two compartments. The cathode has the configuration of stacks of wire mesh screen (or wire cloth). In the conceptual design, electrolytic cells would be inserted between centrifugal contactor stages (ANL-7799, p. 54).

Because the desired process function is the reduction of plutonium ions, which occurs at the cathode of the cell, attention here is limited to cathode performance and design. Since no difficulties are expected with

the anodic reaction (formation of oxygen gas from dilute nitric acid), this reaction is not discussed.

In order to relate design parameters to the fraction of plutonium reduced in each pass through the cathode chamber, a simple model relating cell design parameters was developed. This model follows a standard chemical engineering approach for design of steady-state flow reactors, viz., a material balance over an element of volume at a position x along the length L of the cathode chamber of a cell. A schematic of the electrolytic cell is shown in Fig. V-1. This chamber has a uniform superficial cross-sectional area A. The surface area of the cathode is assumed to be distributed evenly within the volume of the chamber at a constant surface area per unit volume, $S_V$. As the catholyte flows from the inlet along the length of the cathode chamber, the reaction proceeds and C (the concentration of the ion species being reduced) decreases.

The material balance is written for a constant-cross-section electrolytic cell over the differential element of length. On the assumption that an irreversible first-order heterogeneous chemical reaction occurs, the balance is as follows:

(flow rate) · (differential change of ion concentration) = (rate coefficient) · (concentration driving force) · (cathode surface area)

Or, as symbols:

$$V_F \cdot dC = - k_L \, C \, S_V \, A \, dx \qquad (1)$$

where the variables are defined as follows:

$V_F$ = volumetric flow rate

$C = C(x)$ = concentration of species (i.e., Pu-IV) being reduced, at point x along flow path

A = superficial cross-sectional area of cathode chamber

$k_L$ = specific rate constant (with units of linear velocity)

For the case in which the inlet Pu(IV) concentration $C_1$ and the outlet Pu(IV) concentration $C_2$ differ little, the variables can be related directly by an average value of C as follows:

$$\text{reduction rate} = k_L \, C_{av} \, S_V \, AL = V_F(C_1 - C_2) \qquad (1A)$$

For the general case where $C_1/C_2$ is substantially greater than unity, the variables are properly related by integrating eq. 1 as follows:

$$-\int_{C_1}^{C_2} d \ln C = \int_0^L \frac{k_L \, S_V \, A \, dx}{V_F}$$

$$2.3 \log \frac{C_1}{C_2} = \frac{k_L \, S_V \, AL}{V_F} \qquad (2)$$

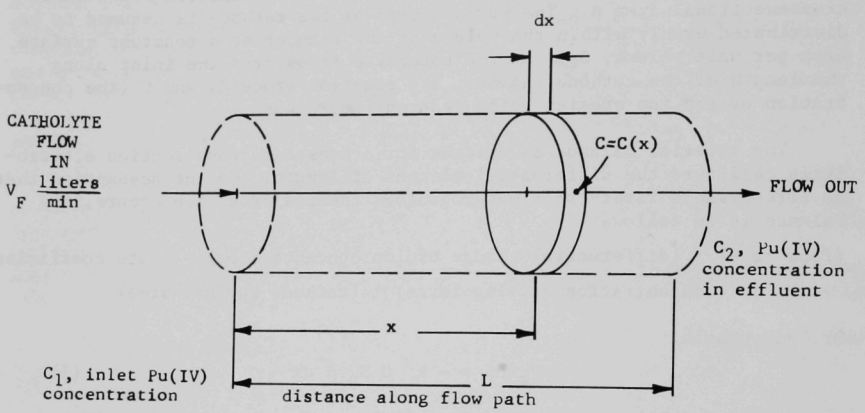


FIG. V-1. Diagram for Model of Continuous Electrolytic Cell

Certain parameters may be derived directly from the above definitions as follows:

$u$ = superficial linear velocity = $V_F/A$

$S$ = total surface area of cathode = $S_V$ AL

$T$ = residence time in reductor = $S/(S_V V_F)$

$L_{1/2}$ = cathode length for reduction of 50% of plutonium =

$$\frac{0.69\ V_F}{k_L\ S_V\ A} = \frac{0.69u}{k_L\ S_V}$$

$S_{1/2}$ = cathode area for reduction of 50% of plutonium = $\dfrac{0.69\ V_F}{k_L}$

$T_{1/2}$ = residence time for reduction of 50% of plutonium =

$$\frac{0.69}{S_V\ k_L} = \frac{L_{1/2}}{u}$$

$S_{1/100}$ = cathode area for reduction of 99% of plutonium = $\dfrac{4.6\ V_F}{k_L}$ .

In this simple model, $k_L$ can be considered a purely empirical constant as in the analysis of experimental results presented below (Table V-1) or, if the electrochemical reduction and the flow of electrical current are controlled by mass transfer, k can be immediately identified as a mass-transfer rate coefficient. In either case, the current density i (current flux) at the cathode surface at point x is given by $k_L$ C(x) or, more exactly, by the expression 16.1 n $k_L$ C for an n-electron transfer.

It should be noted that this simplified model is subject to certain limitations, the most important of which are as follows:

(a) Electrode field effects on ion transport are assumed to be negligible. This assumption is true only for the case of an indifferent electrolyte, i.e., an electrolyte with a high concentration of nonreacting ions, so that solution conductivity due to nonreacting ions is much greater than that due to the reacting ions. This condition is closely approximated in the present case (hydrogen ions, the principal carriers of current, are not converted to hydrogen gas at the cathode).

(b) Although $k_L$ is dependent on the linear velocity (u), the feed rate $V_F$, the cell geometry, solution properties, etc., this dependence is not shown in this model. The dependence of $k_L$ on flow variables is discussed in a later section.

This model was used to make an empirical analysis of the performance of two very different electrochemical cells[1,2] that had been used to reduce $U^{+6}$ to $U^{+4}$ in dilute nitric acid solution. The performance of these two cells and that of the ANL conceptual electrolytic cell could be compared because of the generally similar chemical systems. The major difference

is that reduction of plutonium (IV) to plutonium (III) is a one-electron reversible reaction (rather than a two-electron irreversible reaction), which occurs at a slightly lower half-cell potential.

One electrochemical cell[1] was a large plate-type unit tested at Savannah River Laboratory. This unit represented a very rugged semiworks design, with plates stacked in a filter-press arrangement to give six cells electrically connected in series and with the liquid catholyte flowing through the cells in parallel. The cell parameters and some performance data are given in Table V-1. This cell was used for batch operations by recycling the electrolyte from a large storage tank through the cell for several hours. The fraction converted per pass was small.

A small cell with a wire-mesh cathode was operated by the British investigators Finlayson and Mowat,[2] also to reduce $U^{+6}$ to $U^{+4}$ in nitric acid solutions. They constructed a cell with the catholyte flowing in series through modular units to give overall high single-pass conversions in a flow (rather than a batch) system. In order to obtain a large cathode surface area, tantalum wire mesh was used for the cathode. In each unit, liquid flowed axially through a wire-filled cathode chamber having the form of a cylindrical annulus. The inner diameter of the cathode was formed by the diaphragm--a cylindrical tube of PORVIC which is a brand of microporous polyvinyl chloride having a pore size of 5 μm. The major reason for preference of this material was its low resistivity compared with that of sintered glass and certain unspecified ion-exchange membranes. As many as seven units were tested in series to give 99.8% conversion to U(IV) at a flow rate of 1 liter/hr. Overall operating data and design parameters for this cell are shown in Table V-1.

From conversion data reported for each of the seven modular units of the British cell, values of $k_L$ were calculated for successively lower uranium (VI) concentrations and tabulated in Table V-2. These values verify the assumption that $k_L$ is independent of concentration. The $k_L$'s so determined could be used to design cells to give other conversion efficiencies.

The preliminary design concept of a wire-screen cathode cell, presented previously by Krumpelt (ANL-7799), was used to calculate design parameters (also shown in Table V-1). (This is only an illustrative initial concept and should not be taken as a reference design.) In the calculations, the volumetric flow rate and mass rate of reduction were chosen to conform to a conceptual Purex flowsheet for production rates up to about 500 kg plutonium/day (80% plant factor). Several such electrolytic cells would be used in conjunction with a bank of centrifugal contactors.

In later sections of this report, other designs of a wire-screen cell and a plate cell are presented for this reference flowsheet case.

## B. Design Principles

### 1. Review of Dependence of Mass Transfer on Flow Conditions

A discussion in the preceding report in this series (ANL-7799, pp. 55-57) is the basis for the assumption that plutonium reduction rate and cell current are controlled by mass transfer (i.e., rate of diffusion

TABLE V-1. Calculated Cell Parameters

from Experimental and Estimated Data

| Cell Parameter | Type of Cell | | |
|---|---|---|---|
| | Stacked Plates[a] | Annular Mesh Cathode[b] | Baffled-Screen Cathode[c] |
| Volumetric Flow Rate, $V_F$, liters/min | 540 | 0.0167 | 11.0 |
| Mass Rate of Reduction, g-mol/sec | 0.069 | $5 \times 10^{-5}$ | 0.033 |
| $C_1$, Concentration of Species at Inlet | 1.3M U | 0.50M U | 0.18M Pu |
| Total Current, A | 24,000[d] | 36 | 3200 |
| Current Efficiency, % | 55 | 74 | 100[e] |
| u, Superficial Linear Velocity, ft/sec | 4.4 | 0.0005 | 0.65 |
| Fraction Reduced in Single Pass | 0.0055 | 0.998 | 0.50 |
| T, Residence Time, min | 0.015 | 132 | 0.27 |
| S, Total Cathode Surface Area, $ft^2$ | 30 | 8.5 | 8.9 |
| Total Cell Volume, liters | 8.1 | 2.2 | 3.0 |
| $S_V$, Cathode Area/Cell Volume, $cm^{-1}$ | 3.1 | 4.1 | 2.8 |
| Diaphragm Area/Cathode Area | None[f] | 0.55 | 0.10 |
| Av. Cathode Current Density, $A/cm^2$ | 0.86 | 0.0046 | 0.40 |
| $k_L$, $\frac{\text{g-atom } U^{+6}}{(\text{min})(ft^2)(\text{M } U^{+6})}$ | 0.10 | 0.0092 | -- |
| $k_L$, $\frac{\text{g-atom Pu}^{+4}}{(\text{min})(ft^2)(\text{M Pu}^{+4})}$ | -- | -- | 0.85 |

[a] SRL semiworks cell.[1] The $k_L$ for this cell was the average rate during the initial hour of operation.

[b] British cell.[2]

[c] Krumpelt, ANL-7799, The cell parameters and $k_L$ are estimated for 60-mesh screen of wire of approximately 7-mil diameter.

[d] 4000 amperes through 6 cells in series.

[e] Assumed.

[f] No diaphragm was used, but in this type of cell, a diaphragm would have a diaphragm area to cathode area ratio of 1.0.

TABLE V-2. Variation of $k_L$ Calculated from British Data[2] for Several Modules (catholyte flow connected in series)

Electrolytic Reduction: U(VI) to U(IV)
Nominal Flow = 1 liter/hr
Nominal Inlet Concentration: 0.5M U
Seven Identical Cells with Flow Connected in Series
Cathode Surface per Cell = 1300 $cm^2$ (est.)

| Modular Unit | % of Feed Converted to U(IV) at Module Exit | % of Feed Converted in Module | $k_L$ [g-atom/(min)$(ft^2)$(M)] | Current (A) | Current Efficiency (%) |
|---|---|---|---|---|---|
| 1 | 32 | 32 | 0.0053 | 9 | 96 |
| 2 | 64 | 32 | 0.0076 | 9 | 96 |
| 3 | 76 | 12 | 0.0047 | 5 | 64 |
| 4 | 88 | 12 | 0.0082 | 5 | 64 |
| 5 | 94 | 6 | 0.0082 | 3 | 54 |
| 6a | 99 | 5 | 0.021 | 3 | 48 |
| 7a | 99.8 | 0.8 | 0.019 | 2 | 13 |
| Overall | 99.8 | -- | av. 0.0092 | 36 | av. 74 |

[a]The temperature of these cells was raised to 60°C by applying heat, and the catholyte was stirred by rotating the anode compartment.

of plutonium ions from the bulk of the solution to and from the cathode surface). Quantitative relations are developed in the following discussion after a brief review of mass-transfer and electrochemical technology.

The general treatment by Bennett and Myers[3] of those principles of the transport process that are common to mass and heat transfer is used for the engineering design. These relationships are supplemented by McAdams' detailed summary[4] of heat transfer (because heat transfer analogies can be used to predict mass transfer behavior). The more theoretical approach of Hinze[5] on the subject of turbulence helps to define the limited contributions of theory and the points that require experimental validation.

The classic paper of Chilton and Colburn[6] establishes the empirical basis of the mass-transfer/heat-transfer analogy in terms of dimensionless groups of variables termed j-factors. These factors are based on hydrodynamic model theory applied to standard configurations and are used to define formulas for empirical correlations. The basic nomenclature and formulas are given in Table V-3. The main point of Table V-3 is the mass transfer/heat transfer analogy, which allows mass-transfer rates to be predicted from heat-transfer data.

Subsequent experimental mass-transfer work to confirm the correlations for standard configurations was done by Linton and Sherwood,[7] using a dissolution technique to measure mass transfer rates. This work indicated that the standard correlations gave calculated $k_L$ values that were equalled or exceeded by experimental values, thus being "safe" in practical design. However, this work was limited in scope and does not furnish the best basis for our designs.

Less experimental data is available on mass transfer than on heat transfer. Moreover, even heat-transfer data on flow normal to cylinders and wires over a wide range of diameters is limited to the heterogeneous collection of data given by McAdams,[4] which is not as clear-cut as desired for a design basis. The only modern experimental work on flow over wires is that of Piret[8] on heat transfer to water, which work uses correlations of the type

$$\frac{hD}{k} = a\left(\frac{Du\rho}{\mu}\right)^{m}\left(\frac{Cp\ \mu}{k}\right)^{1/3}$$

where a and m are numerical constants. The discussion of Piret shows that correlations of this form cannot be expressed with constant a and m over a wide range of the Reynolds number. Experimenters who report a constant m = 1/2 have done so on the basis of data obtained for the slope $\Delta h/\Delta Re$ for a limited range of D; often, correlations against Re of several orders of magnitude are reported for a single D.

2. Mass Transfer from Wires

Experimental data on mass transfer rates as a function of velocity are not available from the literature for small-diameter cylinders and wires. The validity of extrapolation from large-diameter measurements of either mass transfer or heat transfer coefficients is questionable, and dependence has been placed on the work of Piret,[8] who obtained correlations on heat transfer from water to small wires. Confidence that for a single

TABLE V-3. Nomenclature Used in Dimensionless Groups of Variables for Correlations Common to Heat Transfer and Mass Transfer[3,6,12]

| Dimensionless Groups | Variables |
|---|---|
| Reynolds number = $\frac{Du\rho}{\mu}$ = Re | Cp heat capacity, Btu/(lb)(°F) |
| Prandtl number = $\frac{Cp\ \mu}{k}$ = Pr | D diameter (length), ft |
| Nusselt number = $\frac{hD}{k}$ = Nu | $D_L$ mass diffusion coeff.,[a] $ft^2$/sec |
| Sherwood number = $\frac{k_L D}{D_L}$ = Sh | h heat transfer coeff., Btu/(sec)($ft^2$)(°F) |
| Schmidt number = $\frac{\mu}{\rho D_L}$ = Sc | k thermal conductivity, Btu/(sec)($ft^2$)(°F/ft) |
| friction factor = f/2 | $k_L$ mass transfer coeff., ft/sec[b] |
| | u linear fluid velocity, ft/sec |
| | $\frac{k}{Cp\ \rho} = \alpha$ = thermal diffusivity,[a] $ft^2$/sec |
| | $\mu$ = viscosity, lb/(sec)(ft) |
| | $\rho$ = density, $lb/ft^3$ |
| | $\frac{\mu}{\rho} = \nu$ = kinematic viscosity,[a] $ft^2$/sec |

j-factor

Heat transfer, $j_H = Nu\ Re^{-1}\ Pr^{-1/3} = \phi_H(Re)$

Mass transfer $j_D = Sh\ Re^{-1}\ Sc^{-1/3} = \phi_D(Re)$

ANALOGY: $\phi_H(Re) = \phi_D(Re) = f/2$

$$Sh\ Re^{-1}\ Sc^{-1}\ Sc^{2/3} = Nu\ Re^{-1}\ Pr^{-1}\ Pr^{2/3}$$

$$\left(\frac{k_L}{u}\right)\left(\frac{\mu}{\rho D_L}\right)^{2/3} = \left(\frac{h}{\rho Cpu}\right)\left(\frac{Cp\ \mu}{k}\right)^{2/3}$$

[a] Note similar units for analogous transport processes.

[b] The complete set of dimensions for $k_L$ are mass/(time)(surface area)(mass/volume)--see text.

cylinder, the j factor for mass transfer equals the j factor for heat transfer is based on a review of key references presented above and Piret's own discussion.

Piret's general correlation was:

$$\frac{hD}{k} = 0.965 \left(\frac{Du\rho}{\mu}\right)^{0.28} \left(\frac{Cp\ \mu}{k}\right)^{0.3}$$

where the solution properties are taken near the wire surface.

The accuracy of Piret's correlation was evaluated with the dimensional formula:

$$h = (0.28\ T_F + 3.86) \times 10^{-5}\ \frac{u^{0.28}}{D^{0.72}}$$

where $T_F$ is the arithmetic average of wire and water temperatures, °F. In this form, the probable error in h is $\pm$3.4%, for the range $0.1 < Re < 10$.

While Piret's work seems the soundest and most applicable of available experimental work, he used wire of only two sizes (1 mil and 2.6 mils) and linear velocities in the range $0.009 < u < 0.45$ ft/sec. It would seem desirable to obtain additional evidence that the wire diameter has indeed the same effect on hD/k as the linear flow velocity.

From the data for a 2.6-mil diameter wire and a velocity of 0.390 ft/sec, an h of 1.477 Btu/(sec)(ft$^2$)(°F) was calculated. From the equation for j-factor analysis in Table V-3, using $D_L = 5.8 \times 10^{-6}$ cm$^2$/sec and $\alpha = 1.50 \times 10^{-3}$ cm$^2$/sec, $k_L$ is 0.695 g-mol/(min)(ft$^2$)(M) (i.e., 0.747 cm/min or $4.08 \times 10^{-4}$ ft/sec) for these conditions. The value of $k_L$ at other fluid velocities and wire diameters is proportioned according to $k_L \propto u^{0.28}/D^{0.72}$.

The applicability of Piret's correlation to the data for the British cell cannot be established because wire-mesh data are lacking. The fact that Piret's correlation states that the exponent for velocity is low ($k_L \propto u^{0.28}$) could be favorable for a low pressure drop during operation. As the fluid velocity is reduced, $k_L$ drops relatively much less than does the pressure drop ($\Delta P$), which correlates as $\Delta P \propto u^2$ in the turbulent range and $\Delta P \propto u$ in the streamline range.

The previous estimate for a 7.5-mil wire (made by another correlation for mass transfer) was $k_L = 0.85$ g-mol/(min)(ft$^2$)(M), as entered in the third column of Table V-1. For the same conditions, $k_L$ calculated by Piret's formula is somewhat smaller, namely, $k_L = 0.37$ g-mol/(min)(ft$^2$)(M). Variations of this sort between different empirical correlations indicate the need for experimental tests as a basis of cell design. Optimization of residence time and pressure drop, which are very critical in cell operation, will be controlled by the relationship of $k_L$, u, and D.

3. Mass Transfer from Plates

The work of Lin et al.[9] establishes the basic correlations for

mass transfer in an electrochemical cell for flow within a channel (in this case, a cylindrical annulus). Their work shows that measurement of limiting current densities in electrolytic oxidation-reduction reactions is a convenient technique for establishing fundamental mass-transfer relationships.

Krishna et al.[10] followed up Lin's work in a very practical way. They promoted turbulence by adding a packed bed of spheres in the annulus, increasing $k_L$'s by a factor of 10. In other work, stirring also has been shown to promote mass transfer in flow over cylinders and wires.[11,12]

For a plate-type cell, the basic design concept uses the "standard configuration" of liquid catholyte flowing through a channel having a "thin" rectangular cross section, i.e., a small dimension of ~1/8 in. This small dimension is the distance between the diaphragm and the cathode and is also the path of current flow.

Mass transfer in this cell is from the bulk of the flowing solution to a large wall surface (the cathode) of the channel. For this configuration, the basic flow regime is the same as for cylindrical annuli, and so the work of Lin et al. on diffusion-controlled electrode reactions is the chief source of practical design principles.

Lin found that mass transfer in his tests was correlated very well as $k_L$ in both streamline and turbulent flow with standard correlations. Our interest is in the turbulent case:

$$j_D = \frac{k_L}{u} \left(\frac{\mu}{\rho D_L}\right)^{2/3} = f/2$$

where f/2 for an annulus is given by

$$f/2 = 0.023 \left(\frac{De\ u\rho}{\mu}\right)^{-0.2}$$

with the equivalent diameter $De = D_2 - D_1$. Lin's data, for $325 < Sc < 3110$ and $2100 < Re < 30{,}000$, have an average deviation of ±4.9% and a maximum deviation of ±15.5%. The accuracy of this work by Lin using electrolytic oxidation-reduction seems superior to the results of Linton and Sherwood[7] using dissolution methods.

Using the above correlation with flow data from Table V-1, together with estimated solution properties, we may calculate $k_L$ for the SRL plate reactor.[1] The calculated $k_L$ is 0.19 g-atom/(min)(ft$^2$)(M), which is about a factor of two larger than the empirical value $k_L = 0.1$ g-atom/(min)(ft$^2$)(M) in Table V-1. The discrepancy is expected because the SRL reactor was operated without a diaphragm and the net efficiency of reduction was lower.

Lin's formula above may be rearranged to give

$$k_L = 0.023 \frac{u^{0.8}}{De^{0.2}} \left(\frac{\mu}{\rho}\right)^{0.2} \left(\frac{\mu}{\rho D_L}\right)^{-2/3}.$$

Lin's cell shows a stronger dependence of $k_L$ on u than do wire-type cells.

The work of Krishna and Rao[10] with an annulus packed with small spheres was done with the same general equipment and method as Lin's work (in fact, Krishna[10] made explicit comparison with Lin's work). Krishna's correlation used a Re defined as:

$$Re = \frac{D_p u_o \rho}{\mu},$$

where $D_p$ is the diameter of the spherical packing and $u_o$ is the superficial linear velocity. Since the void fraction for the packed spheres was 0.41, the superficial linear velocity is related to the average linear velocity of the liquid in the interstices by the equation $u = u_o/0.41$. The ratios of $k_L$ for the packed and nonpacked cases as a function of Re are as follows (appropriately defined for the nonpacked case with an average u):

| $\frac{De\ u\rho}{\mu}$ (no packing) | $\frac{k_L\ (packed)}{k_L\ (nonpacked)}$ |
|---|---|
| 1550 | 10 |
| 4670 | 10 |
| 9350 | 9.1 |
| 17,400 | 7.5 |

Thus for Re = 8440 of the SRL case, the $k_L$ would be improved by a factor of about 9.4. The above values were based on a plot of Krishna's[10] data. An analysis of Krishna's data by linear regression resulted in the following correlation of $j_D$ vs Re:

$$j_D = 0.82\ Re^{-0.38} \quad (3 < Re < 1400)$$

These data are for two sizes of spherical packing, 0.074-in. dia and 0.192-in. dia. The standard error of the regression, $\sigma_{y \cdot x}$, was about 6% of the mean $j_D$.

4. Diaphragm Design

The function of a diaphragm in an electrolytic cell is to prevent transfer of the cathode solution to the anode (where reoxidation occurs). In practice, cell diaphragms consist of rigid partitions with holes or pores that allow the passage of cell current by ionic conduction without gross movement of solution between the anode and cathode compartments. The diaphragm thus becomes a special cell component that offers a resistance to current flow and contributes a particular voltage drop across the cell. If this voltage drop is kept low, electrode potentials can be effectively controlled and excessive heat is not generated in the cell.

a. A Simple Calculational Model for Diaphragm Conductance

If it is assumed that the cell current must pass through the free openings in the diaphragm by ionic conductance, the current density, i, based on the superficial area of the diaphragm is given by

$$i = \frac{I}{S_d} = F\left(\frac{\Delta V}{\Delta x}\right) \sum_i (\lambda_i c_i),$$

where

$I$ = total cell current, A

$S_d$ = superficial area of the diaphragm, $cm^2$

$F$ = fraction of $S_d$ that is the effective cross-sectional area for ionic conductance

$\Delta V$ = voltage drop across the diaphragm, V

$\Delta x$ = thickness of the diaphragm, cm

$\lambda_i$ = ionic conductance of ion i, $(cm^2)(ohm^{-1})/(g\ equiv.)$

$c_i$ = concentration of ion i $(g\ equiv)/(cm^3)$

The above dimensions balance by virtue of the following equivalence:

$$A = V \cdot ohm^{-1}.$$

In the present calculation of ionic conductance through the diaphragm, it is assumed that only $H^+$ and $NO_3^-$ ions are carrying current. Although $OH^-$ ions are present, their concentration is very low. Plutonium ions have an equivalent conductance about 10 percent that of $H^+$, but the contribution of plutonium would be small at low plutonium concentrations and is neglected here.

Since in the above expression for current density at the diaphragm, the ionic conductance, $\lambda_i$, is a function of both the temperature and the concentration, it is necessary for purposes of design to consider the effect of these variables. A temperature of 45°C was selected as representative of practical cell temperatures; conductivity increases with increasing temperature. The dependence of $\lambda_i$ on concentration can be expressed for $H^+$ and $NO_3^-$ by means of the ratio $\lambda_i/\lambda_o = 1 - 0.250\ \underline{M}^{1/2}$, where $\lambda_o$ is the equivalent ionic conductance at infinite dilution and $\underline{M}$ is the molarity of the ion. Also, by the additive property of the ions $\lambda_{H^+} + \lambda_{NO_3^-} = \Lambda_{HNO_3}$ (see Robinson and Stokes,[13] especially pp. 148, 372, 465). Thus the formula for the diaphragm conductance can be written:

$$i = F\,\frac{\Delta V}{\Delta x}\,(1 - 0.250\ \underline{M}^{1/2})\ 0.550\ \underline{M},$$

where $\underline{M}$ is the molarity of nitric acid. This approximation is believed to be accurate to within ±10% for $\underline{M} < 6.0$.

b. Calculation of Typical Current Densities for Diaphragms

In order to achieve high conductivity, F should be as large

as possible, and $\Delta x$ should be as small as possible. Clearly, considerations of mechanical structure impose practical limits here. It is estimated that the most favorable practical values of F and $\Delta x$ are F = 0.40 and $\Delta x$ = 0.076 cm. For these values of F and $\Delta x$, current densities were calculated for various values of $\Delta V$ and $HNO_3$ molarity as follows:

| $HNO_3$ (M) | $\Delta V$, (V) | i, ($A/cm^2$) |
|---|---|---|
| 1.0 | 10.0 | 22 |
| 1.0 | 1.0 | 2.2 |
| 0.10 | 1.0 | 0.27 |
| 0.010 | 1.0 | 0.028 |
| 5.0 | 1.0 | 6.8 |

Apparently, current densities (flux) at the diaphragm of the order of 1 $A/cm^2$ are achievable if favorable diaphragm dimensions can be used and there is moderate ionic conduction (in this case, due to acidity). For a voltage drop of $\sim$1.0 V across the diaphragm, the heat generated in the cell would increase appreciably and adequate cooling would be required.

From Table V-1, it is seen that for ratios of diaphragm area to cathode area between 1/10 and 1, the cathode current densities were as high at 0.40 $A/cm^2$. Since the total current flowing through the diaphragm is the same as the current through the electrodes, smaller diaphragm areas result in larger current densities at the diaphragm.

c. Structural Materials for Diaphragms

Diaphragms of porous plastic and porous ceramic have been used and reported in the literature. A small laboratory cell at SRL[1] used a very thin porous ceramic diaphragm; the British cell[2] used a microporous polyvinyl chloride. Ceramic material was too fragile in the acceptably thin and porous form, and was unobtainable in larger sizes.[14] In the absence of experimental tests, the long-term use of porous polyvinyl chloride in nitric acid at temperatures likely to be encountered in a cell is questionable. Other plastics such as polyethylene, polypropylene, and silicone material (G-7 resin) are similarly questionable. The requirement that the diaphragm material resist attack by organics is another factor to consider. Teflon apparently has generally superior properties in this application to a cell diaphragm; excellent technical data are available for Teflon. Glass cloth or fiber laminates greatly enhance the structural properties of Teflon sheet and are readily available. It has been assumed that material having closely spaced perforations would be preferable to sintered porous material because the perforated material would be practical with higher values of $F/\Delta x$ in the preceding equation.

In the selection of material for this application, the wetting behavior of the material would be very important. If wetting were not complete, the effective cross section would be much reduced, resulting possibly in unacceptably high electrical resistance. However, it has been reported by duPont that Teflon is wet by acetic acid, hexane, and

triethanolamine (among others), and so it may be possible to attain proper wetting of Teflon. If a perforated sheet is selected, it could be designed to function in the absence of wetting by using larger holes. Experimental tests are expected to settle these questions.

Although plutonium ions can diffuse through a diaphragm, it is believed that plutonium diffusion would be small in practice because of relatively low plutonium concentrations in the nitric acid solution. In flow systems, control of pressure drop across the diaphragm may be necessary. Such control could prevent plutonium diffusion through the diaphragm if a pressure drop were selected that caused liquid flow to oppose the diffusion of plutonium ions under the prevailing concentration gradient.

d. General Considerations of Conductivity of Solutions

The relation above for ionic conductance in an acid solution

$$i = F\left(\frac{\Delta V}{\Delta x}\right) (1 - 0.250\ \underline{M}^{1/2})\ 0.550\ \underline{M}$$

indicates that there will be a voltage drop $\Delta V$ across any portion of the current path $\Delta x$ where current is carried only by ionic conduction; that is, where ions are not carried by convectional flow or turbulent mixing. In other words, in those portions of the cell where there is well-developed flow or good mixing, high cell currents without high voltage drop can be expected. The interelectrode spacing will not be important under conditions of good mixing of bulk electrolyte, and large $\Delta V$ will occur only at stagnant boundary layers adjacent to the diaphragm and at the electrode surface itself.

Since voltage drop is inversely related to mixing efficiency, the use of a conductivity cell to measure the efficiency of mixing is possible. A standard cell for this purpose would measure total cell current for a given overall $\Delta V$. Current would vary with transport effectiveness in a mixing chamber located between the two diaphragms, one diaphragm at each electrode.

5. Pressure Drop

Pressure drop for catholyte flow can be calculated by methods indicated in the Chemical Engineer's Handbook[15] for a packed bed of spheres and for a wire screen.

Packed Bed (Ref. 15, p. 5-50)

$$\text{head loss, ft fluid/ft length} = \frac{\Delta P}{\rho L} = \frac{2\ u_o^2}{g_c D_p}\ \frac{(1 - \varepsilon)^{1.9}}{\varepsilon^3}$$

where $u_o$ = superficial linear velocity, ft/sec

$\varepsilon$ = void fraction

$D_p$ = dia of spherical packing, ft

$g_c$ = gravity constant, 32.2 $\frac{\text{lb-ft}}{(\text{lb force})(\text{sec}^2)}$

Wire Screen (Ref. 15, p. 5-35)

$$\text{head loss, } \Delta h, \text{ ft (fluid)} = \Delta h = \frac{u_o^2}{2\, g_c} \left(\frac{1 - \alpha^2}{\alpha^2}\right) \frac{n}{c^2}$$

where n = number of screens

$\alpha$ = projected fraction of open area of screen

$$c^2 = 0.01 \quad \frac{D_s u_o \rho}{\alpha\, \mu} \quad , \text{ for } \frac{D_s u_o \rho}{\alpha\, \mu} < 100$$

($D_s$ = aperture width, ft)

$$c^2 = 1, \text{ for } \frac{D_s u_o \rho}{\alpha\, \mu} \geq 100.$$

The effect of these relationships on cell design can be summarized thus:

1) for beds of packed spheres, $\varepsilon$ is nearly constant (usually $\varepsilon$ is $\sim$0.4) and hence $\Delta P \propto u_o^2 D_p^{-1}$. This is as expected for turbulent flow.

2) for the wire screens, approximately,

$$\Delta h \propto n\, u_o^2 \left(\frac{1 - \alpha^2}{\alpha^2}\right)$$

at Reynolds numbers of 100 or more; this is as expected for orifice flow, since $u_o^2 \left(\frac{1 - \alpha^2}{\alpha^2}\right)$ is a kinetic loss factor. For a smaller $D_s$, $\Delta h$ is proportionately higher for a given u, as indicated by the case for Re < 100. For screens of higher mesh number and smaller aperture, $\alpha$ is smaller and $\Delta h$ is higher.

C. Conceptual Design of a Plate Cell

In order to illustrate the favorable design possible for a plate-type cell, the following design is used to achieve 50% reduction of a 0.18M $Pu^{+4}$ feed solution with a volumetric rate of 11 liters/min. This corresponds to the reference flowsheet for a production rate up to ~500 kg Pu/day. There is a 1/8-in. spacing between cathode and diaphragm. This space is packed with a single layer of 1/8-in. dia Pyrex spheres. The superficial liquid velocity $u_o$ is 0.24 ft/sec. The Reynolds number, based on the packing diameter of 0.125 in., is 84; the void fraction $\varepsilon = 0.476$. The superficial cross-sectional area is 25.0 $cm^2$.

From the above pressure-drop correlation for packed beds

$$\frac{\Delta P}{\rho L} = 0.94 \frac{\text{ft (head)}}{\text{ft (length)}} .$$

The estimate of $k_L$ is obtained from the correlation $j_D = 0.82\ Re^{-0.38}$ (above) for $Re = \frac{D_p u_o \rho}{\mu} = 84$ as follows:

$$j_D = 0.15 = \frac{k_L}{u_o} \left(\frac{\mu}{\rho D_L}\right)^{2/3} \quad \text{for } D_e = 0.125 \text{ in.}$$

$$k_L = 0.32 \text{ cm/min;}$$

$$S_V = 6.58 \text{ cm}^{-1} \text{ (for the assumed cell configuration)}$$

Residence time, $T_R = \frac{0.69}{(0.0324)(65.8)} = 0.33$ min = 20 sec

Length of cathode in direction of liquid flow, L = (0.24 ft/sec)(20 sec) = 4.8 ft

Volume = (11 liters/min)(0.33 min) = 3.6 liters (liquid holdup)

Overall pressure drop = $\frac{\Delta P}{\rho}$ = 6.2 ft (liquid head)

Cell width = $\frac{25.0 \text{ cm}^2}{0.125 \text{ in.}} \frac{\text{in.}^2}{6.4 \text{ cm}^2} = 44.3$ in. = 2.7 ft

Approximate overall cell dimensions:

rectilinear slab, 1.5 in. thick, 3 ft wide, 5 ft long.

This slab configuration is favorable for geometric control of criticality. Diaphragm area is equal to cathode area, which is (4.8 ft)(2.7 ft) = 13.0 $ft^2$ = 12,000 $cm^2$. The current density (flux) at the cathode and diaphragm is $\frac{3200}{11700} = 0.27$ A/$cm^2$.

D. Conceptual Design of a Wire-Screen Cell

The following specifications exemplify a favorable design of a wire-screen cell based on the general configuration presented previously by Krumpelt (ANL-7799). That cell configuration has been modified slightly on the basis of engineering considerations and $k_L$ has been calculated on the basis of Piret's data. A diagram of the configuration of the cathode segment of a cell is shown in Fig. V-2.

The wire diameter chosen was 7.5 mils, formed in a square mesh of 32 per in. The openings in the screens and the spacing between screens were each 24 mils. This rather small opening and close spacing was selected to illustrate the advantages of using a fine wire screen in obtaining a compact cell at low pressure drop. Thirty-two screens are placed together in a stack in this design. Rods of 1/4-in. diameter are included (Fig. V-2) to promote turbulence and to increase $S_V$, the surface-to-volume ratio.

$$S_V = 9.6 \text{ cm}^{-1}$$

$$S_A = 1.50 = \frac{\text{total wire surface area in screen}}{\text{superficial area of screen}}$$

$$D_s = 24 \text{ mils} = \text{separation between wires in screen}$$

$$\alpha = 0.52 \text{ (see section B.5 above)}$$

The fluid velocity $u_o$ is 0.10 ft/sec and $k_L$ is 0.237 cm/min, derived from Piret's data. A is 60 $cm^2$. Total cathode surface area, $\frac{0.69\ V_F}{k_L}$ is 32000 $cm^2$. The Reynolds number is 35.6.

$$\text{surface area of one screen} = (1.50)(0.60) = 90 \text{ cm}^2$$

$$\text{number of screens, } n = \frac{32000}{90} = 356$$

$$\text{number of stacks of 32 screens} = 356/32 = 11$$

The total volume of catholyte in this unit is 11(60 $cm^2$)(5.5 cm) = 3.6 liters. The total pressure drop across the screens is only 0.42 ft (head), in contrast to 6 ft calculated for the plate cell; the small additional pressure drop due to flow in other parts of the cell was not calculated. The cathode chamber is a rectilinear slab with overall dimensions of 2.2 in. by 4.7 in. by 22 in. The small dimensions of the cathode chamber serve to provide geometric control for criticality. The overall dimensions of the entire cell are estimated to be approximately $\frac{5}{2}$ in. by 5 in. by 2 ft. The total surface area of the diaphragm is 1320 $cm^2$. For the specified current flow of 3200 A, the current flux at the diaphragm is $\frac{3200}{1320}$ = 2.4 A/$cm^2$.

In this cell design estimate, the uncertainty of the principal design parameters, $k_L$ and $\Delta P$, is believed to be fairly high, about a factor of two. Therefore, selection of an optimum design should be used on experimental tests.

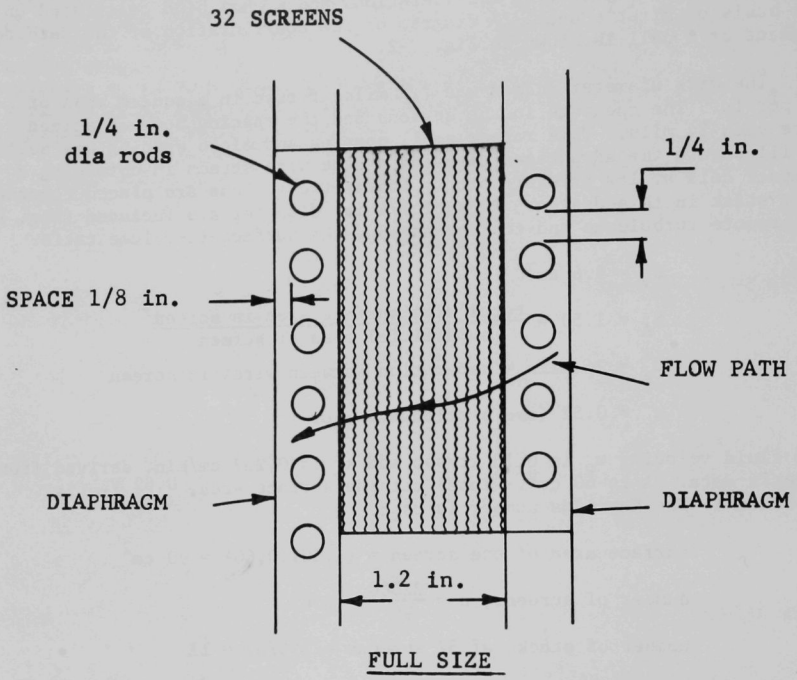


FIG. V-2. Configuration of Cathode Segment

(flow normal to screens)

## E. Suggestions for Further Work

In design estimates made so far, only approximate solution properties at certain assumed temperatures were considered. A closer look at the detailed behavior of important properties over a range of temperatures is required for optimization.

A preliminary review of the literature disclosed that a power supply consisting of controlled a-c voltage applied through a stepdown transformer and a dry rectifier system is favored at the present state of the art. In a three-phase system of half-wave rectifiers, the output d-c voltage[16] ripple is only 18%. Further examination should be made as to whether additional reduction of ripple is required.

Proposed components should be tested with respect to mass transfer behavior, pressure drop, voltage drop, and materials compatibility.

## REFERENCES


1. G. Starr Nichols, Electrolytic Preparation of Uranous Nitrate, USAEC report DP-1065 (Aug. 1966).

2. M. B. Finlayson and J. A. S. Mowat, Electrolytic Reduction of Uranium (VI) and Plutonium (IV) Nitrate Solution: Development of a Continuous Process, Electrochem. Technol. 3(5-6), 148 (1965).

3. C. O. Bennett and J. E. Myers, Momentum, Heat, and Mass Transfer, McGraw-Hill, New York (1962).

4. W. H. McAdams, Heat Transmission, 3rd Ed., McGraw-Hill, New York (1954). McAdams' graph is also printed in ANL-7799, p. 67.

5. J. O. Hinze, Turbulence, McGraw-Hill, New York (1959).

6. T. H. Chilton and A. P. Colburn, Mass Transfer Coefficients, Ind. Eng. Chem. 26(11), 1183 (1934).

7. W. H. Linton, Jr., and T. K. Sherwood, Mass Transfer from Solid Shapes to Water in Streamline and Turbulent Flow, Chem. Eng. Prog. 46, 258 (May 1950).

8. E. L. Piret, W. James, and M. Stacy, Heat Transmission from Fine Wires to Water, Ind. Eng. Chem. 39, 1098 (Sept. 1947).

9. C. S. Lin, E. B. Denton, H. S. Gaskill, and G. L. Putman, Diffusion-Controlled Electrode Reactions, Ind. Eng. Chem. 43(9), 2136 (Sept. 1951).

10. M. S. Krishna and C. Venkata Rao, Mass Transfer in Packed Annular Cells, Chem. Age India (Bombay) 18(1), 41 (1967).

11. M. S. Krishna and G. J. V. Jagannadhraju, Ionic Mass Transfer in Agitated Vessels: Part I, Indian J. Technol. 3, 263 (1965).

12. E. J. Cairns and A. M. Breitenstein, The Transport of Hydrogen to Cylindrical Anodes in Stirred Electrolytes, J. Electrochem. Soc. 114(4), 349 (Apr. 1967).

13. R. A. Robertson and R. H. Stokes, Electrolyte Solutions, 2nd ed., Butterworths, London (1959).

14. G. Starr Nichols, Savannah River Laboratory, private communication (1971).

15. W. H. Perry, Chemical Engineer's Handbook, 4th ed., McGraw-Hill, New York (1963).

16. Mark's Standard Handbook for Mechanical Engineers, 7th ed., p. 15-120, McGraw-Hill, New York (1967).

B